EFFECT OF SURFACE ROUGHNESS ON TENSILE PROPERTIES OF ADDITIVELY MANUFACTURED THIN-WALLED STRUCTURES

by
Abdul Vahap YOĞURTÇUOĞLU

Submitted to the Graduate School of Engineering and Natural Sciences
in partial fulfilment of the requirements for the degree of
Master of Science

Sabancı University

December 2022

ABSTRACT

EFFECT OF SURFACE ROUGHNESS ON TENSILE PROPERTIES OF ADDITIVELY MANUFACTURED THIN-WALLED STRUCTURES

Abdul Vahap YOĞURTÇUOĞLU

Master of Science in Manufacturing Engineering, December 2022

Thesis Supervisor: Prof. Dr. Bahattin KOÇ

Keywords: Surface Roughness, Thin Wall, LPBF, Tensile Properties, Additive Manufacturing

Additive manufacturing (AM) has enabled manufacturing of complex geometries that are infeasible to produce with conventional manufacturing methods. Among the AM methods, laser powder bed fusion (LPBF) has gained significant attention from various industries due to its ability to fabricate components with intricate details. With LPBF processes, it is possible to manufacture functional lightweight components with thin walls and internal features that may not be accessible for secondary surface finishing operations. However, due to the nature of the process, AM produces undesirable surface quality, especially on the down-facing surfaces of inclined walls, which can negatively impact mechanical performance. In this study, thin-walled Cobalt-Chrome (CoCr) test samples were manufactured through LPBF with varying build angles and thicknesses to investigate the influence of surface roughness on tensile properties. The produced surface textures were analysed, and the areal surface roughness metrics were quantified. The effects of process parameters such as wall thickness, build angle, and angle of the laser incidence on the surface roughness were investigated. Tensile tests were conducted on both as-built samples and their machined counterparts, and the results showed that the negative impact of surface roughness becomes less significant as sample thickness increases. Analysis of Variance (ANOVA) was used to identify the most influential surface roughness metrics on tensile properties. According to the ANOVA results, while

Sv, S10z, and Sku were the most influential parameters on ultimate tensile strength, Sa, Sq, Sv, and S10z was found to be significant for effective modulus.

ÖZET

YÜZEY PÜRÜZLÜLÜĞÜNÜN EKLEMELİ İMALAT İLE ÜRETİLEN İNCE CİDARLI YAPILARIN ÇEKME ÖZELLİKLERİ ÜZERİNDEKİ ETKİSİ

Abdul Vahap YOĞURTÇUOĞLU

Üretim Mühendisliği Yüksek Lisans Tezi, Aralık 2022

Tez Danışmanı: Prof. Dr. Bahattin KOÇ

Anahtar Kelimeler: Yüzey Pürüzlülüğü, İnce Cidarlı Yapılar, Toz Yataklı Eklemeli İmalat, Çekme Özellikleri, Eklemeli İmalat

Eklemeli imalat, geleneksel imalat yöntemleriyle üretilmesi mümkün olmayan karmaşık geometrilerin üretilmesini mümkün kılmıştır. Eklemeli imalat yöntemleri arasında, özellikle lazer toz yatağı füzyonu (LPBF), yüksek çözünürlüklü ve ince ayrıntılara sahip bileşenler üretebilme kabiliyetinden dolayı birçok endüstriden büyük ilgi görmüştür. LPBF teknolojisinin getirdiği tasarım esnekliği, ince cidarlı iç kanalar içeren fonksiyonel hafif bileşenlerin üretilmesi için kullanılmıştır. Ancak, bu bileşenlerin iç kanallara sahip olması yüzey iyileştirme uygulamaları için engel teşkil etmektedir. Eklemeli imalatın doğası gereği, özellikle eğimli duvarların aşağı bakan yüzeylerinde gözlenen düşük yüzey kalitesi mekanik performansı olumsuz etkileyebilmektedir. Bu çalışmada, yüzey pürüzlülüğünün çekme özellikleri üzerindeki etkisini araştırmak amacıyla değişen basım açıları ve duvar kalınlıkları ile ince cidarlı Kobalt-Krom (CoCr) çekme testi örnekleri üretilmiştir. Üretilen yüzeyler, analiz edilip alansal yüzey pürüzlülük parametreleri ölçülmüştür. Duvar kalınlığı, basım açısı ve lazer açısı gibi üretim parametrelerinin yüzey pürüzlülüğü üzerindeki etkileri araştırılmıştır. Yüzey karakterizasyonundan sonra, pürüzlü numuneler ve bunların işlenmiş muadilleri için çekme testleri gerçekleştirilmiş ve sonuçlar, numune kalınlığı arttıkça yüzey pürüzlülüğünün olumsuz etkisinin daha limitli hale geldiğini ortaya koymuştur. Çekme özellikleri üzerinde en etkili yüzey pürüzlülük parametrelerini belirlemek amacıyla ANOVA testi kullanılmıştır. ANOVA

sonuçlarına göre UTS üzerinde en etkili parametreler Sv, S10z ve Sku iken, efektif modül için Sa, Sq, Sv ve S10z parametrelerinin etkili olduğu görülmüştür.

ACKNOWLEDGEMENTS

I would like to thank my thesis advisor Prof. Dr. Bahattin Koç for his guidance and all the support he provided during my master's education. I always felt his interest and support, through the master thesis period. By sharing his deep knowledge and experience during the thesis process, he provided great academic guidance for producing fast and effective solutions to emerged problems. As his student, I feel very lucky to have the privilege of working in such a respectful and supporting environment.

I would like to thank Assoc. Prof. Sezer Özerinç and Asst. Prof. Bekir Bediz, who made constructive and instructive comments by being a jury member in my master thesis defense, for their valuable opinions and contributions.

I would like to thank my colleague and my friend Dr. Uğur Şimşek for helping me during the thesis period and for all his contributions.

I would like to thank my dear mother, Müzeyyen Yoğurtçuoğlu, and my dear sister, Hande Umay Küren, for embracing me with affection, for always being there for me, and for their unwavering support and love.

I would like to thank my father Ercan Yoğurtçuoğlu for his endless love and faith in me.

I sincerely thank Merve Irmak Ayazoğlu for being by my side during the most stressful times, keeping me away from hopelessness and pessimism, giving me hope and encouraging me with her love and support.

TABLE OF CONTENTS

LIST OF TABLES

LIST OF FIGURES

LIST OF ABBREVIATIONS

2D	Two Dimensional
3D	Three Dimensional
AM	Additive Manufacturing
ANOVA	Analysis of Variance
ASTM	American Society for Testing and Materials
CAD	Computer Aided Design
CT	Computed Tomography
DS	Down Skin
DoE	Design of Experiment
EBM	Electron Beam Melting
EDM	Electrical Discharge Machining
FEA	Finite Element Analysis
FV	Focus Variation
ISO	International Organization for Standardization
LPBF	Laser Powder Bed Fusion
SLM	Selective Laser Melting
SLS	Selective Laser Sintering
Stl	Standard Triangle Language
PCC	Pearson Correlation Coefficient
US	Up Skin
UTS	Ultimate Tensile Strength

1. INTRODUCTION

Due to recent advances in digital manufacturing technology, metal additive manufacturing, specifically laser powder bed fusion (LPBF), has garnered significant attention from various industries, including aviation, automotive, energy, and biomedical sectors. (Blakey-Milner, et al., 2021) (DebRoy, et al., 2018) (Selema, Ibrahim, & Sergeant, 2022). Laser powder bed fusion (LPBF) or also called selective laser melting (SLM) is a powder bed fusion technology enables to manufacture multiple complex parts with intricate details on the same platform simultaneously. LPBF provides numerous advantages by using entire working volume of the machine, reducing manufacturing time and raw material consumption (Sendino, Gardon, Lartategui, Martinez, & Lamikiz, 2020; Covarrubias & Eshraghi, 2018). LPBF process provides design flexibility trough enabling production of complex geometries and internal features which are either difficult or impossible to manufacture with conventional manufacturing methods. This design flexibility also enables fabrication of lightweight parts which are crucial especially in the automotive and aerospace industry (DebRoy, et al., 2018).

Many aerospace applications have internal features that may be inaccessible, therefore they rely on as-build surfaces produced by AM process. Due to design complexity of the additively manufactured components, surface finishing is not possible for some features and such regions can be left in as-build condition. While LBPF offers many aforementioned benefits, it produces components with poor surface quality, which can negatively impact mechanical properties (Herzog, Seyda, Wycisk, & Emmelmann, 2016) (Emmelman, Kranz, Herzog, & Wycisk, 2016) (Obilanade, Dordlofva, & Törlind, 2021). Therefore, a detailed evaluation of surface roughness metrics and their effect on the mechanical characteristics of as-built components is necessary. The recent increase in

the use of AM metals has highlighted the need to understand the surface features caused by the powder bed fusion process.

Definition of the most frequently adopted surface roughness metrics are presented in ISO specification standards ISO 4287 and ISO 25178-2 (ISO 4287, 2000; ISO 25178-2, 2012). The ISO 4287 profile parameter Ra, which is the arithmetic mean of the absolute ordinate values within a sampling length, was identified by Townsend et al. as the most used texture parameter in both industry and academia (Townsend, Senin, Blunt, Leach, & Taylor, 2016). Besides the profile texture parameters, area texture parameters become more prominent for characterization of the AM surfaces. By the nature of the additive manufacturing, AM surfaces have three-dimensional features with irregular patterns. The areal surface roughness metrics provide advantages over profile texture parameters with the ability to capture the three-dimensional surface features. Sa is the most commonly used areal texture parameter which is the arithmetic mean height of the defined area (Townsend, Senin, Blunt, Leach, & Taylor, 2016). There have also been a number of studies that analyzed the effectiveness of mean surface roughness metrics in representing the AM surfaces and reported that other surface metrics may have an impact on the mechanical characteristics as well (Arola & Ramulu, 1999; Gockel, Sheridan, Koerper, & Whip, 2019).

The effects of surface roughness on the mechanical properties of AM components are widely studied in the literature, with a majority of the studies focusing on the effects on the fatigue behavior of structures. Gockel et al. investigated the effects of Sa (arithmetic mean height) and Sv (maximum pit height) on the fatigue life of alloy 718 round bars produced through LPBF process and found that the Sv is inversely correlated with the fatigue life (Gockel, Sheridan, Koerper, & Whip, 2019). Sneddon et al. used Ra parameter to characterize Ti64 surfaces and concluded that the fatigue life of the tested specimens decrease as the specimen Ra increases (Sneddon, et al., 2020).

A limited number of studies have investigated the effect of surface roughness on the tensile properties of structures. Algardh et al. manufactured thin-walled Ti6Al4V specimens through electron beam melting (EBM) and found that the tensile properties of thin-walled structures can be dominated by variations in Ra values of the surface textures (Algardh, et al., 2016). Everhart et al. compared as-build titanium specimens to their machined counterparts in terms of tensile properties and found that unfinished Ti-6AL-

4V round bars had lower ultimate tensile strength (UTS) and yield strength (Everhart, Sawyer, Neidt, Dinardo, & Brown, 2016).

There are few studies in the literature that have evaluated the mechanical properties of AM components considering the effect of surface roughness. Yang et al. highlighted the challenges of fabricating thin-walled structures (Yang, et al., 2019). These challenges of fabricating thin-walled structures could be the reason for the lack of studies in this area. The objective of this study is to investigate the effects of areal surface roughness metrics and sample thickness on the effective elastic modulus, yield strength, and ultimate tensile strength (UTS) values of thin-walled CoCr samples produced through LPBF. The effects of build thickness, build angle, and sample position with respect to the laser focal location on the surface texture of the fabricated specimens will also be examined. The main aim of this study is to provide an overview of the significance of surface roughness metrics on the required tensile properties for thin-walled structures.

2. LITERATURE REVIEW

In the following sections, additive manufacturing process will be described to provide a better understanding of the technology. After that, the definition of surface roughness and standard roughness metrics will be presented. In addition, the surface characteristics of the additively manufactured samples will be summarized. Lastly, the effect of surface roughness metrics on various mechanical properties will be discussed based on related literature. The studies investigated the fatigue life, tensile properties and mechanical performance of the thin-walled structures will be reviewed in the last section.

2.1 Additive Manufacturing

According to ISO/ASTM 52900 (ISO/ASTM 52900 standard, additive manufacturing (AM) is defined as “process of joining materials to make parts from 3D model data, usually layer upon layer, as opposed to subtractive manufacturing and formative manufacturing methodologies”. Unlike conventional subtractive manufacturing techniques, AM produces parts the layer-by-layer deposition of raw material, typically in powder or wire form. This manufacturing method uses a focused heat source to selectively melt or fuse the raw material to produce the final geometry.

AM reduces material waste due to its ability to fabricate complex shapes and internal features that are either difficult or impossible to produce with conventional manufacturing methods (Whip, 2018). This design flexibility enables fabrication of

lightweight parts which is particularly important in the automotive and aerospace industries (Wong & Hernandez, 2012).

Additive manufacturing is a broad term that encompasses various manufacturing methods. These methods can be classified into three categories: powder bed systems, powder feed systems, and wire feed systems (Frazier, 2014). This classification can be further refined based on the specific characteristics of each AM method. In this research, powder bed fusion method is used for additively manufacturing the sample tests and hence explained below.

Additive manufacturing begins with a 3D CAD model oriented in a build volume and sliced with planar planes by the layer thickness used. The LPBF process creates a part by laying down powder material along the sliced layers and fusing the material with a laser source, layer by layer, within an inert chamber. (DebRoy, et al., 2018). Figure 1 shows a schematic representation of a LPBF process.

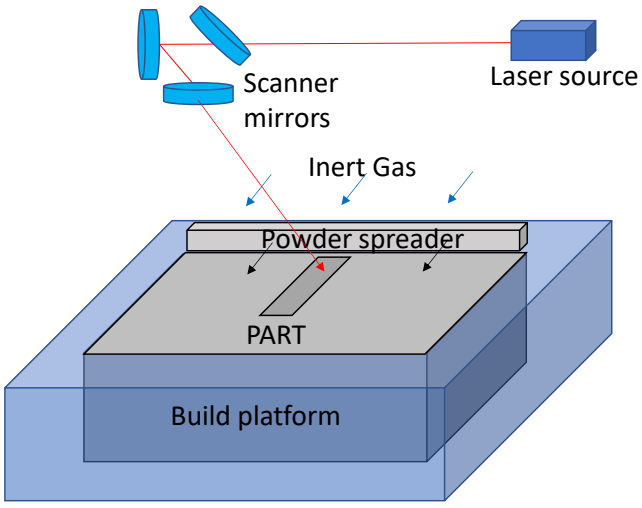

Figure 1: Schematic representation of the LPBF process

In addition to LPBF, there are other powder bed fusion technologies that use different types of heat sources. The electron beam melting (EBM) process uses an electron beam heat source within a vacuumed environment. The EBM technology relies on two step sequence, first the heat source lightly sinters the powder particles, and the process follows by the fusion of the sintered particles (DebRoy, et al., 2018). Selective laser sintering (SLS) and selective laser melting (SLM) processes use a laser heat source. The difference

between these two processes is that the SLS applies heat to sinter the particles without melting where the SLM utilizes a higher heat to completely melt the powder (Wong & Hernandez, 2012). Each of these LPBF technologies has its own advantages and disadvantages compared to other AM methods. In this study, the SLM method was used to manufacture thin-walled tensile specimens.

2.2 Surface Roughness

Surface topography refers to the geometric information of a surface form and its features. Surface roughness metrics are quantifications of these surface features, calculated using a characterization of the surface topography (Townsend, Senin, Blunt, Leach, & Taylor, 2016). One of the major limitations of additive manufacturing is the poor surface quality produced by AM technologies, which often falls below industry standards. In terms of component functionality, surface quality is a critical property because it can affect part failures (Shubhavardhan, et al., 2021). Surface roughness of AM components can be improved through post-processing, but for some applications with internal features that are not accessible for surface enhancement, the mechanical performance may depend on the as-build surface condition. Therefore, a thorough surface characterization is crucial for AM components with as-build surfaces (Obilanade, Dordlofva, & Törlind, 2021).

ISO specification standards ISO 4287 and ISO 25178-2 include definitions of the most commonly used surface roughness metrics (ISO 4287, 2000) (ISO 25178-2, 2012). ISO 4287 provides terms, definitions, and parameters for profile measurements, while ISO 25178-2 develops the terminology, concepts, and parameters for areal surface texture. These standard surface roughness metrics, their definitions, and the formulas for the areal metrics are provided in Table 1. The letter “R” represents 2D profile, while the letter “S” represents 3D areal roughness metrics. In addition to these metrics, the “S10z” parameter was also evaluated, which corresponds to the arithmetic mean of the ten highest (Sz) values along the measurement area.

Table 1: Definitions of surface roughness metrics

Metric	Definition of Roughness Metric	Equation
Ra / Sa	Arithmetical Mean Height	$Sa = \frac{1}{A}\iint_A \lvert Z(x,y)\rvert dxdy$
Rq / Sq	Root-mean Square Height	$Sq = \sqrt{\frac{1}{A}\iint_A \lvert Z^2(x,y)\rvert dxdy}$
Rsk / Ssk	Skewness	$Ssk = \frac{1}{Sq^3}\left[\frac{1}{A}\iint_A \lvert Z^3(x,y)\rvert dxdy\right]$
Rku / Sku	Kurtosis	$Sku = \frac{1}{Sq^4}\left[\frac{1}{A}\iint_A \lvert Z^4(x,y)\rvert dxdy\right]$
Rp / Sp	Maximum Peak Height	$Sp = \max z(x,y)$
Rv / Sv	Maximum Pit Height	$Sv = \lvert\min z(x,y)\rvert$
Rz / Sz	Maximum Height	$Sz = Sp + Sv$

A surface profile is shown in Figure 2 to define the geometrical meanings of the surface roughness metrics. The geometric interpretation of the areal surface roughness metrics can be made similarly to the profile metrics, considering an area rather than a 2D profile.

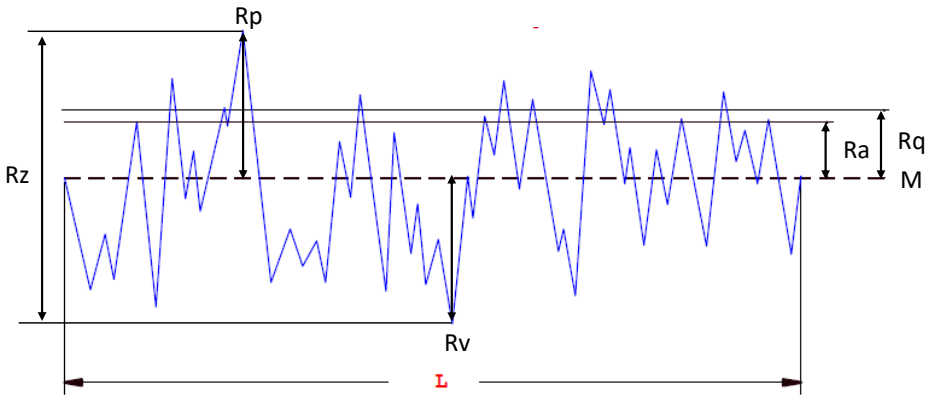

Figure 2: Surface roughness metrics explained on a 2D surface profile

Rsk/Ssk and Rku/Sku parameters gives insight about the shape of the surface texture. Skewness describes the level of symmetry of the surface heights about the mean plane. The sign of the skewness indicated either predominance of peaks (Ssk >0) or valleys (Ssk<0) (ISO 25178-2, 2012). The sharpness of the distribution is explained by the

kurtosis parameter. The surface height distribution becomes spiked when the Sku is greater than three and becomes flat when Sku is less than three (ISO 25178-2, 2012). Figure 3 explains the skewness and kurtosis parameters on a 2D surface profile. A surface texture with normal distribution would have Ssk equal to 0.00 and Sku equal to 3.00 (Lee, Rasoolian, Silva, Pegue, & Shamsei, 2021).

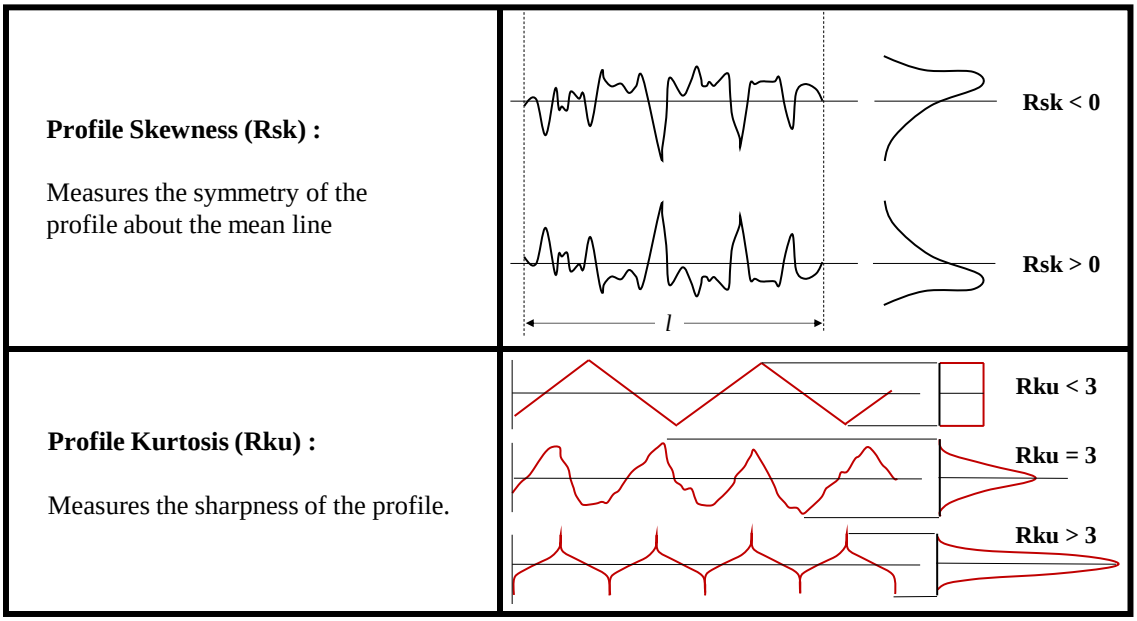

Figure 3: Explanation of skewness and kurtosis parameters *(Herring, Mardel, & Fox, 2010)*

The surface finish of additively manufactured parts is difficult to control due to melt tracks, un-melted particles, and melt pool extensions. The nature of the process can also lead to metallurgical defects such as balling, ripple effect, or hump-like structures, porosities, and surface cracks, which contribute to the poor surface quality of AM components (Shubhavardhan, et al., 2021). The formation of these defects and the surface quality of additively manufactured structures are influenced by various factors, including process parameters that can affect the surface quality during the melting and solidification of the metal powders. Many studies have investigated the effects of laser power, scan speed, and hatch distance on the surface roughness of additively manufactured samples (Covarrubias & Eshraghi, 2018; Tian, Tomus, Rometsch, & Wu, 2017; Charles, Elkaseer, Thijs, Hagenmeyer, & Scholz, 2019). Eidt et al. studied the influence of processing

parameters on the surface roughness of vertical and inclined surfaces and showed that the surface roughness improved with increasing laser power (Eidt, et al., 2019).

In addition to process parameters, the effects of design parameters such as build angle, layer thickness, and laser incidence angle on surface roughness have also been studied in the literature (Sendino, Gardon, Lartategui, Martinez, & Lamikiz, 2020; Tian, Tomus, Rometsch, & Wu, 2017; Wan, et al., 2020). Tian et al. found that the surface roughness of inclined surfaces improved as the build angle increased (Tian, Tomus, Rometsch, & Wu, 2017). In another study, Wan et al. fabricated thin-walled structures in two different thicknesses and reported that surface roughness increased as the build thickness increased (Wan et al., 2020). (Wan, et al., 2020).

Sendino et al. studied the effect of laser incidence angle and found that surface roughness of the fabricated specimens increased as the samples were located further from the laser focus location (Sendino, Gardon, Lartategui, Martinez, & Lamikiz, 2020). Rott et al. investigated the influence of build orientation in relation to the laser incidence angle on the surface roughness of LPBF parts. They introduced a novel "laser relation angle" parameter to describe the interdependence between surface orientation and laser incidence angle and used it to describe position-dependent surface roughness (Rott, et al., 2020).

In this study, the effects of sample thickness, build angle, and angle of laser incidence on the surface roughness of thin-walled structures produced through LPBF are investigated. A total of 27 thin-walled samples are fabricated with varying build angles (50º, 60º, 70º) and sample thicknesses (.035", .055", .075") with three replicates for each angle-thickness combination. The replicates of the samples are located in different regions of the build platform to capture the effect of the angle of laser incidence. The surface roughness of the printed specimens is measured using the focus variation technique with a surface profilometer, the Alicona™ Infinite-Focus G5 instrument, on the up-skin and down-skin surfaces. The measured surface roughness metrics are analysed using the analysis of variance (ANOVA) procedure in Minitab™ software to determine the influencing parameters and their impacts.

2.3.Surface Metrology

There are a variety of techniques for examining surface texture, and the appropriate one should be chosen based on the requirements of the application. It is important to consider the material and structure of the surface topography when selecting a measurement technology. Most studies in the literature use contact-based probing methods to quantify surfaces (Townsend, Senin, Blunt, Leach, & Taylor, 2016). These methods are based on the physical interaction of the probe and the surface and can be destructive, potentially damaging the stylus or the measurement surface. Contact techniques may also have limitations in terms of accessibility to internal features and the ability to capture valleys and peaks on complex, additively manufactured surfaces (Townsend, Senin, Blunt, Leach, & Taylor, 2016).

X-ray computed tomography (XCT) is a technique that is frequently used to characterize the surface textures of additively manufactured components. It has the ability to capture topographic information at microscale levels (Thompson, Maskery, & Leach, 2016). The surface texture can be transformed into a volumetric data without any limitations imposed by vertical walls or undercuts. The biggest advantage of XCT is its ability to characterize internal surfaces without facing accessibility limitations (Thompson, Maskery, & Leach, 2016). However, the biggest limitation of these measurement techniques is the level of accuracy when capturing the details of highly complex surface topologies.

Metal additive surfaces are highly irregular and consist of complex shapes due to unmelted powder particles stuck on the surface and melt extensions (Senin, Thompson, & Leach, 2017). Non-contact techniques are widely used to characterize the additively manufactured surfaces, with their capability to capture 3D textures of the fabricated complex surfaces. The recent shift to use areal surface roughness metrics instead of 2D profile metrics is driving the adoption of optical measurement technologies. According to Townsend et al., the most used optical measurement technique is the focus variation

(FV) technique(Townsend, Senin, Blunt, Leach, & Taylor, 2016). Figure 4 shows the schematic representation of the FV technique. In this study, all surface roughness measurements were performed with the FV technique.

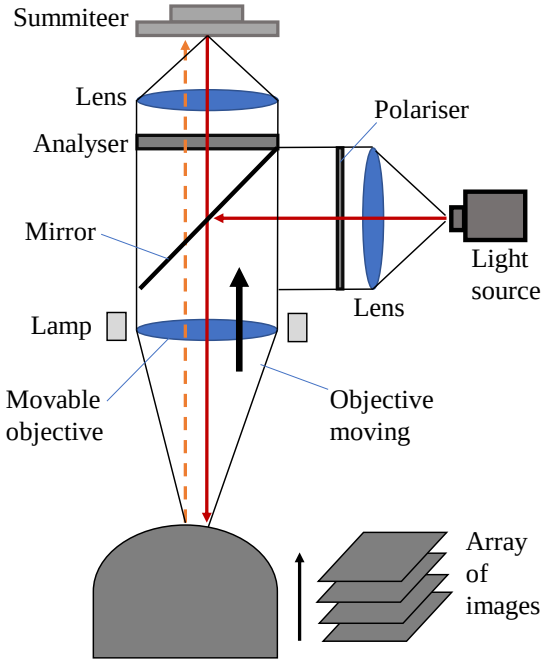

Figure 4: Schematic representation of the focus variation method *(Sredanovic, Globocki-Lakic, Kramar, & Pusavec, 2018)*

2.4 Effect of Surface Roughness on Mechanical Performance of Additively Manufactured Structures

The effects of surface roughness on the fatigue properties of additively manufactured (AM) components have been extensively studied in the literature (Gockel, Sheridan, Koerper, & Whip, 2019) (Lee, Rasoolian, Silva, Pegue, & Shamsei, 2021) (Watring, Carter, Crouse, Raeymaekers, & Spear, 2019) (Pagues, Roach, Williamson, & Shamsaei, 2018) (Zeng, Monu, Lupton, Lin, & Tong, 2020). Gockel et al. investigated the effects of Sa (arithmetic mean height) and Sv (maximum pit height) on the fatigue life of alloy

718 round bars produced through LPBF (laser powder bed fusion) process and demonstrated that Sv is inversely correlated with the fatigue life (Gockel, Sheridan, Koerper, & Whip, 2019). Lee et al. proposed a hybrid surface roughness parameter consisting of Sv, Ssk, and Sku to explain the fatigue behavior of Ti-6Al-4V specimens (Lee, Rasoolian, Silva, Pegue, & Shamsei, 2021). In this study, areal surface roughness metrics of LPBF-produced Ti-6Al-4V specimens were generated according to ISO 4287 to represent a correlation between surface roughness and fatigue life (Lee, Rasoolian, Silva, Pegue, & Shamsei, 2021). Watring et al. reported a difference in fatigue resistance of LPBF-produced Inconel specimens due to surface roughness variations achieved with varying the build angle. Based on quantification using Ra values, it was shown that surface roughness has a significant impact on fatigue life (Watring, Carter, Crouse, Raeymaekers, & Spear, 2019). Pegues et al. showed that crack initiation occurs at the rougher downward-facing surface when fatigue bars are built at an angle, and in general, rougher surfaces (quantified by average roughness, Ra) have a lower fatigue life (Pagues, Roach, Williamson, & Shamsaei, 2018).

Although there has been a number of studies focusing on the relationship between surface roughness metrics and fatigue life performance, there are limited studies in the literature evaluating the impact of surface quality on tensile properties (Everhart, Sawyer, Neidt, Dinardo, & Brown, 2016) (Sneddon, et al., 2020) (Kotzem, Dumke, Sepehri, Tenkamp, & Walther, 2020) (Lebea, Ngwangwa, Desai, & Nemavhola, 2021) (Memu, Hamat, Güleç, & Durlu, 2019). Everhart et al. investigated the effect of surface quality on the mechanical properties of titanium round bars manufactured with electron beam melting (EBM). In this study, tensile test results of the as-built specimens were compared with those of their machined counterparts. It was found that the as-built Ti-6AL-4V round bars exhibited lower ultimate tensile strength (UTS) and yield strength compared to the machined specimens (Everhart, Sawyer, Neidt, Dinardo, & Brown, 2016). In another study, Sneddon et al. examined the effect of surface roughness magnitude and roughness direction on the material failure behavior of titanium alloys manufactured through EBM. They reported that the highest surface roughness value in the maximum tensile stress direction was the most decisive parameter in terms of material failure mechanism (Sneddon, et al., 2020). Kotzem et al. examined the effect of surface roughness on tensile and fatigue properties of Inconel 718 specimens fabricated by EBM. The specimens were tested both in as-built and machined conditions, and it was observed that defect density

and surface roughness (Ra and Rz) had a significant impact on UTS and fatigue strength (Kotzem, Dumke, Sepehri, Tenkamp, & Walther, 2020). Lebea et al. produced dog bone specimens made of Ti-64-ELI with a laser powder bed fusion (LPBF) process and tested them to investigate the effect of surface rough on tensile and fatigue properties. It was shown that the UTS and fatigue life values decreased with increasing Ra, Rsk, and Rq (Lebea, Ngwangwa, Desai, & Nemavhola, 2021).

So far, the aforementioned studies have investigated the effect of surface roughness on the fatigue and tensile properties without taking the size effect into consideration. Only a limited number of studies have examined the influence of wall thickness on the mechanical performance of rough structures (Gathimba & Kitane, 2021) (Hossain, Ghouse, Nai, & Jeffers, 2021) (Algardh, et al., 2016) (Suh, Jung, & Kim, 2010) (Wan, et al., 2020). Gathimba et al. investigated the effects of sample thickness and surface roughness on the tensile properties of corroded steel plates. This study demonstrated that, in combination with sample thickness, the Sa and Sz parameters can have an influence on tensile ductility (Gathimba & Kitane, 2021). In another study, Suh et al. reported that for rolled titanium sheets with similar surface textures, thinner specimens exhibit lower stress-strain curves. Therefore, it was concluded that the effect of surface roughness will increase with decreasing sample thickness (Suh, Jung, & Kim, 2010). A small number of studies have worked with additively manufactured thin-walled structures. Algardh et al. manufactured thin-walled Ti6Al4V specimens through electron beam melting (EBM). This study revealed that the tensile properties of thin-walled structures can be dominated by variations in wall thickness and the Ra values of surface textures (Algardh, et al., 2016). For thin-walled structures fabricated with LPBF, Wan et al. reported thickness and roughness-dependent behaviour in the fatigue strength of Inconel specimens (Wan, et al., 2020).

Even though there has been a significant amount of research focused on the relationship between surface quality and mechanical performance, there are only a few studies that have addressed this relationship for thin-walled structures. This is due to the challenges of fabricating thin-wall structures, which are more sensitive to distortion due to variations in microstructure and melt pool boundaries (Chakraborty, et al., 2022; Yang, et al., 2019). For the design and manufacturing of lightweight components, particularly in aerospace applications, the use of thin-walled structures is crucial, and LBPF technology plays an important role in attaining this goal. In several studies, wall thicknesses up to 5

millimetres (.196 in) considered as thin-walled structures (Chakraborty, et al., 2022; Yang, et al., 2019; Lu, et al., 2021). For the purposes of this study, the thin wall limit is defined as .075 inches, considering design and manufacturing constraints.

Overall, previous studies have mostly focused on the effects of surface roughness on the mechanical properties of nickel, titanium, steel, and aluminum alloys. Many of these samples were produced using the electron beam melting (EBM) process. Cobalt-chromium (CoCr) alloys are widely used in the aviation industry and dentistry due to their high corrosion resistance and advanced mechanical properties such as high stiffness, good fatigue resistance, and tensile strength (Konieczny, Szczesio-Wlodarczyk, Sokolowski, & Bociong, 2020).

However, there is limited research on the effects of surface roughness and sample thickness on the mechanical properties of thin-walled structures produced using the laser powder bed fusion (LPBF) process. This study aims to investigate the effects of areal surface roughness metrics and sample thickness on the effective elastic modulus, yield strength, and ultimate tensile strength (UTS) values of thin-walled CoCr samples produced using LPBF. The aim of this study is to provide an overview of the significance of surface roughness metrics on these tensile properties for thin-walled structures.

3. METHODOLOGY

This section describes the methodological procedures followed in the design, manufacturing, inspection, testing, and statistical analysis processes. First, the design of experiment (DoE) and the strategy followed for build layout planning will be presented. After that, the details of the manufacturing parameters will be explained. In addition, the surface roughness measurement instruments and parameters used will be provided. In the following section, the tensile test setup and testing method will be presented. Lastly, the ANOVA and the statistical analysis procedure will be explained. Figure 5 shows the process map and the equipment used for manufacturing, post-processing, inspection, and testing.

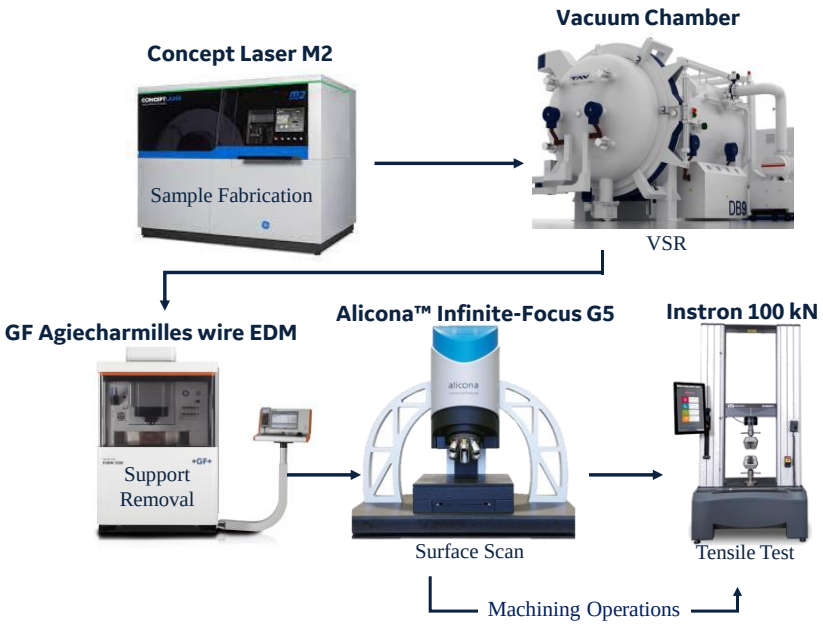

Figure 5: Process map and used equipment for manufacturing, post processes, inspection, and testing

3.1. Experimental Procedure

A design of experiment (DoE) matrix was created to characterize the effects of the design and manufacturing parameters on the surface quality of thin-walled structures and capture the effects of surface quality on the mechanical properties. The aim is to help the designer to keep the surface roughness and surface quality in a certain range to improve material properties such as effective elastic modulus, yield strength and UTS. For this purpose, dog bone specimens measuring 2.40 in length with gauge dimensions of 0.125 in width and 0.620 in length were designed in accordance with the ASTM standard E8 (ASTM Standard E8, 2015). Three different as-build specimens with sample thickness of 0.035, 0.055, and 0.075 inches were chosen to cover variation in mechanical properties with respect to thickness. In addition to as-build specimens, machined dog bone specimens with a minimum machinable thickness of 0.13 inch were also included in the test plan to quantify the offset in the mechanical properties caused by the surface quality. Figure 6 shows the dimensions of as-build and the machined specimens. Machined coupons were designed to have longer grip sections to avoid any slipping during the tensile testing due to their smooth surfaces. As-built specimens have rough surfaces that would naturally provide friction between the grip sections of the coupons and the grippers of the tensile test machine.

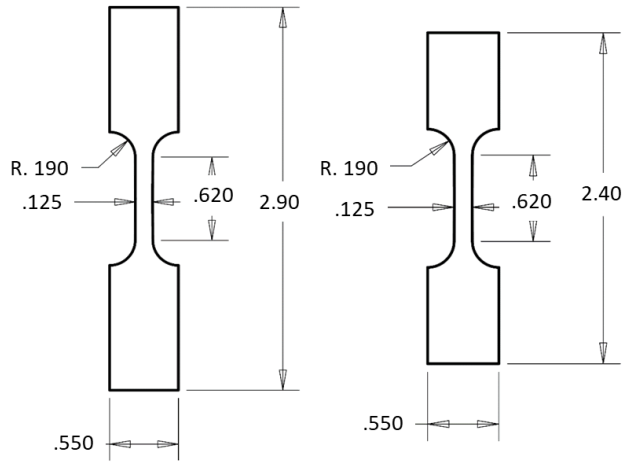

Figure 6: Specimen geometry for mechanical testing in a) machined and b) as-built

To have a variation in surface quality of the as-built specimens and quantify the relationship between the mechanical properties and build-angle, both as-built and machined specimens were placed on the build platform with build angle of 50°, 60° and 70° and the effect of laser incidence angle quantified. Table 2 summarizes the design variables and their level within the proposed DoE. Figure 7 shows the employed build angles with the detail of support structures.

Table 2: Design of Experiment

Variables	Levels		
	-1	0	1
Build Angle (deg)	50	60	70
Sample Thickness (in)	0.035	0.055	0.075
	Interval		
Distance to Laser Focus (in)	0.696 – 6.540		

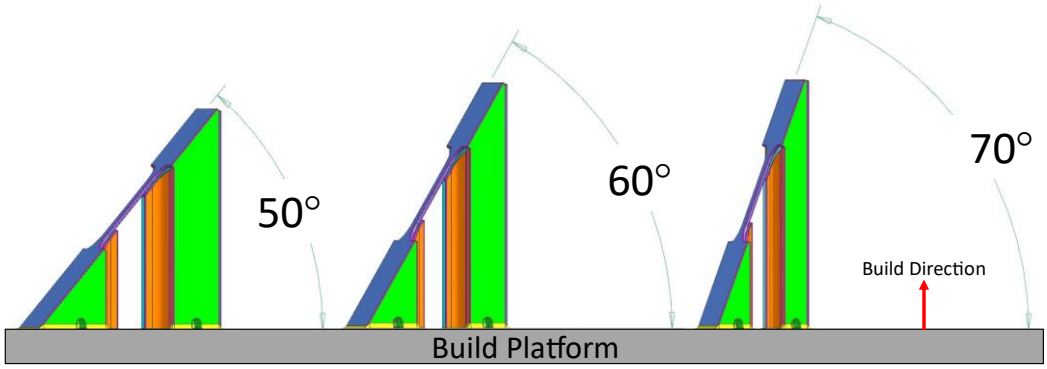

Figure 7: Schematic representation of the build orientations of the specimens; green colour: support structures, blue colour: printed specimens

In accordance with the planned design of experiment (DoE), a total of 27 samples (three for each variable) were built, and 12 extra samples were placed on the build platform to account for failure in the fabrication process and to be used in the test instrumentation. Figure 8 shows the resulting build platform, the failed specimens, gas flow, and recoater directions with the test samples. Three samples which were placed as back-up samples

failed during the manufacturing process due to a build stop. Since the build stop occurred after the gauge sections were fabricated and three replicates for each coupon design were successfully manufactured, the statistical analysis was not affected by the failed samples. In addition, the machined specimens were manufactured in another build platform using the same process parameters. Laser powder bed fusion (LPBF) technology was employed to fabricate the proposed as-built and machined specimens. The test samples made of CoCr were additvely manufactured under an argon gas environment with 180 W laser power, 1500 mm/s scanning speed, and 60 µm hatch spacing parameters using an M2 Concept Laser machine (Gülcan, et al., 2022). The uniform layer thickness was set to 50 µm. A stress relief heat treatment process was applied to the printed specimens. After the building process, the specimens were removed from the build platform by Electrical Discharge Machining (EDM). In order to analyse the surface quality, gauge sections of the manufactured specimens were scanned by a focus variation microscope.

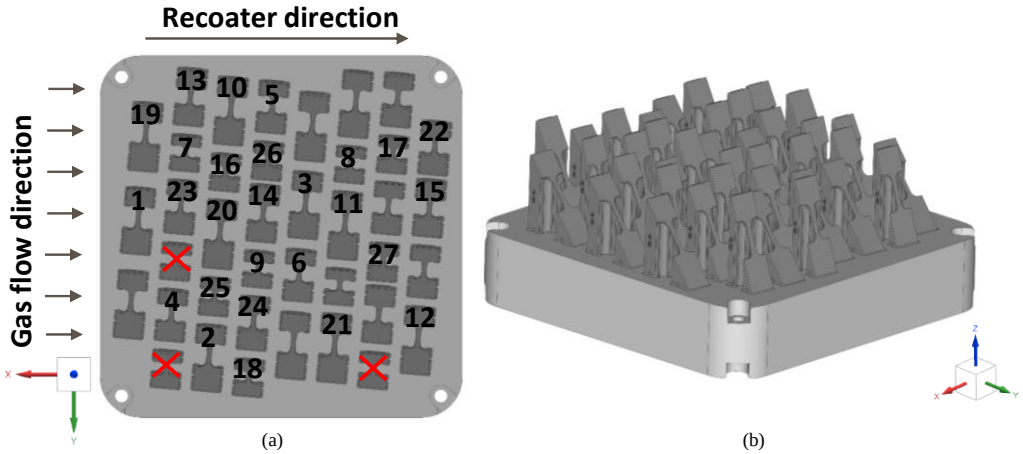

Figure 8: Schematic representation of the specimens on the building platform and laser orientation

Figure 9 shows the position of the laser and and how the laser incidence angle affects parts located in different locations (Sendino, Gardon, Lartategui, Martinez, & Lamikiz, 2020). Hence, the angle of laser incidence varies based on the location of the samples relative to the laser focal point.

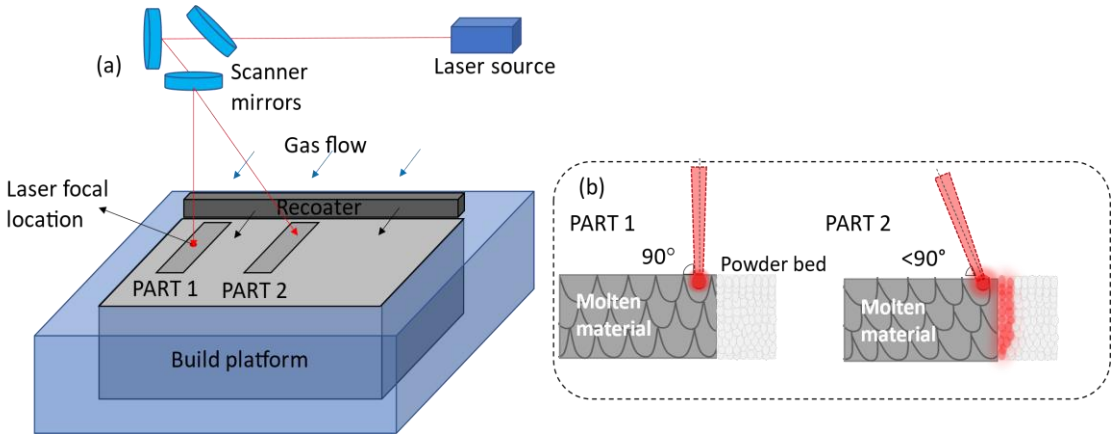

Figure 9: Effect of laser incidence angle: (a) Representation of L-PBF process, (b) Detail of laser incidence angle (Sendino, 2020)

Figure 10 shows the measurement method of the distance to laser focus parameter. The samples included in this study are highlighted in green. The angle of laser incidence is represented by the minimum distance between the center of the gauge section of the specimens and the projected point of the laser focal location onto the build platform. In Figure 10, the red points on the samples indicate the middle points of the gauge sections, and the distance to the laser origin parameter is represented by letter "D".

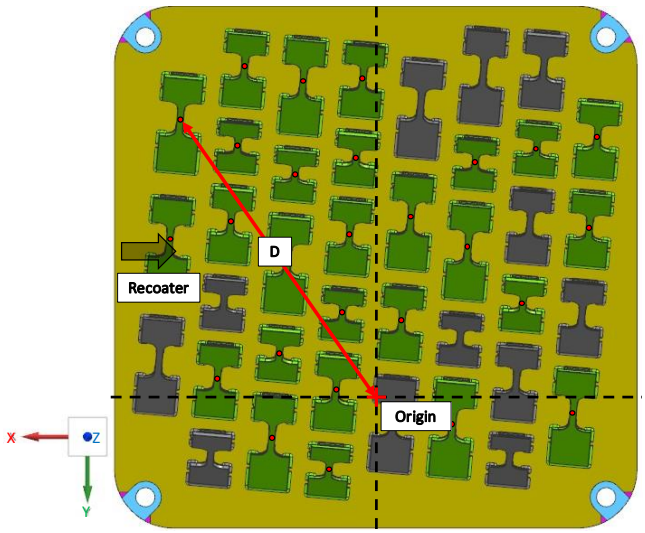

Figure 10: Schematic representation of the specimens on the building platform and laser orientation

3.2. Surface Roughness Measurement

The goal of this study is to quantify the effects of design parameters on the surface texture and the effect of surface roughness on the tensile properties. Therefore, appropriate surface roughness metrics were selected prior to surface characterization. The standard surface roughness metrics according to ISO 25178 were reported and analyzed for the down-skin and up-skin surfaces (ISO 25178-2, 2012).

Once the fabrication process was completed, the specimens were cut from the build plate through electrical discharge machining (EDM). In order to characterize and identify the surface roughness metrics, the entire surface of the gauge section of every specimen was chosen for optical areal measurements and its lengths were used for the cut-off wavelength definition for the profile measurement. All gage section measurements were performed using an Alicona™ optical profilometer. Surfaces were scanned with a 20X objective lens under ring light illumination with 3.51 µm lateral and 12 nm vertical resolutions (Newton, Senin, Chatzivagiannis, Smith, & Leach, 2020). Optical measurements were used to capture a representation of the entire surface and the surface roughness metrics. The surface scanning setup for roughness characterization and the down-skin and up-skin images for a specimen are shown in Figure 11.

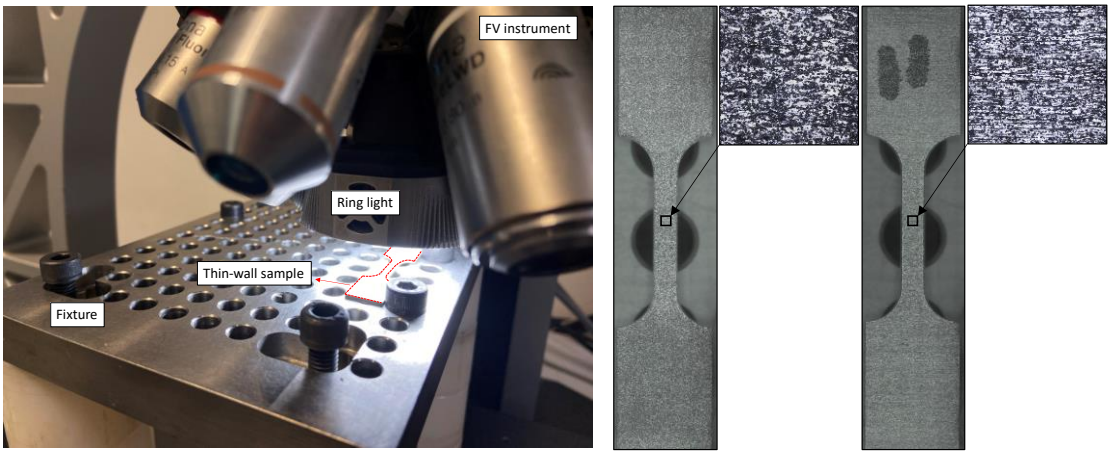

Figure 11: Surface scan of the printed specimens a) Scan set-up, b) Down-skin surface of the as-built specimen, c) Up-skin surface of the as-built specimen

In Figure 12, the scanned area of .060 in^2 from gauge section is shown in green colour. Gaussian filter was applied to the 3D surface texture dataset per EN ISO 11562 (EN ISO 11562, 1996). The surface roughness metrics were calculated by Alicona™ according to EN ISO 4287 with a cut-off length of 0.13 inches (ISO 4287, 2000).

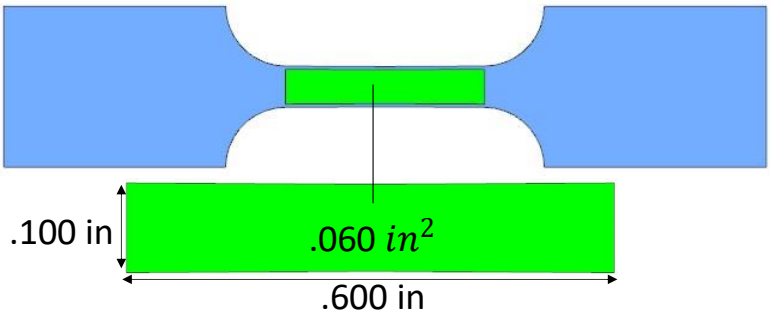

Figure 12: Scanned area of the gauge sections

3.3. Tensile Test

Tensile tests were performed at room temperature using an Instron-100 kN universal electromechanical testing machine at a strain rate of 0.005 in/in/min up to 0.2% yield. After this point, the tensile rate of the head was set to 0.031 in/min until failure. As-built specimens with different build directions and thicknesses and machined specimens were tested. Extensometers were used to measure the strain and calculate the effective elastic modulus, yield, and ultimate tensile strength (UTS). The details of the tensile test setup can be seen in Figure 13.

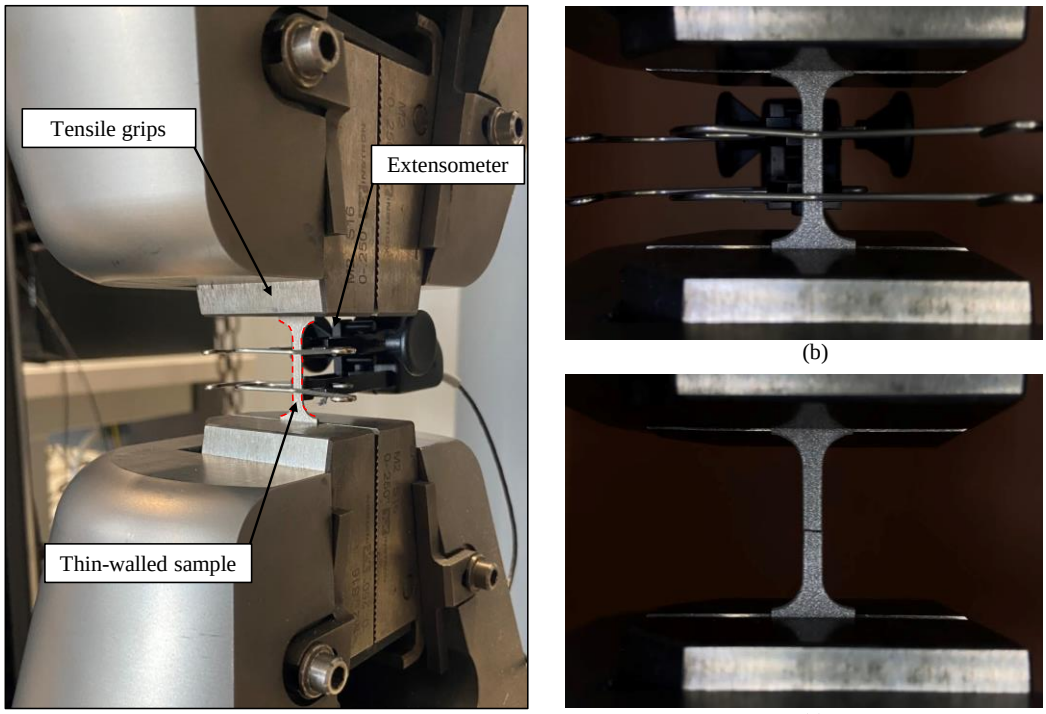

Figure 13: Tensile test of the specimens a) Test set-up, b) Thin-walled specimen before fracture, and c) Thin-walled specimen after fracture

3.4. Analysis of Variance (ANOVA)

Investigating the effect of the build angle, sample thickness, and distance from laser focus on surface roughness was one of the aims of this study. For this purpose, ANOVA was performed to quantify the significance of build orientation (O), sample thickness (T), and distance from laser focus (D) on the arithmetical mean height (Sa) for the down-skin and up-skin surfaces of the gauge section. In the ANOVA procedure, P-value approach is used to determine the significance of the terms. P-values are compared with the predefined alpha value (α=0.05) and the significance criteria is defined as $P \leq \alpha$ (Lee, Rasoolian, Silva, Pegue, & Shamsei, 2021).

In the first step of the ANOVA for the surface roughness, all linear terms of O, T, and D, all square terms (O*O, T*T, D*D), and two-way interaction terms (O*T, D*T, O*D), are employed to analyse the significance of each term in the measured value of surface roughness. Insignificant terms are eliminated from the regression models step-by-step to converge well fitted models for up-skin and down-skin Sa. The results of the ANOVA for the down-skin and up-skin Sa are documented in section 4.3.

Analysis of Variance (ANOVA) was also employed to quantify the correlation between the predefined surface roughness metrics and the tensile properties. Prior to performing a thorough statistical assessment, insignificant roughness metrics were identified and excluded from ANOVA assessments to simplify the statistical analysis and have a better interpretation. For this purpose, Pearson correlation test was first applied first to identify significant surface roughness metrics in terms of tensile properties. The Pearson correlation test measures the linear correlation between two variables and was used for filtering out the insignificant terms before performing ANOVA (Pearson, 1909). P-values were compared with the predefined alpha (α=0.05) value for detecting the significant terms (Montgomery, 2017). Pearson correlation coefficients were also computed for revealing the orders of the correlations. Using the results of the Pearson correlation test, ANOVA was performed with the terms which have P-values less than 0.05 for including the effects of the second order and the interaction terms.

Once the significant surface roughness metrics were determined for each tensile property, separate ANOVA processes were established for elastic modulus, yield, and UTS. All linear, square, and two-way interaction terms of the selected surface roughness metrics were initially included as the input variables into the regression models. Significance of the terms were detected based on the aforementioned P-value criterion and the surface roughness metrics that have no or limited impact on the tensile properties were excluded in the following ANOVA assessment. This process was carried out repeatedly until a strong correlation between the remaining surface metrics and the tensile properties was attained (Ghorbani, Li, & Srivastava, 2020). The correlation test and the ANOVA was performed in the Minitab™ software. The ANOVA and the Pearson correlation test results are presented in the section 4.3.

4. RESULTS AND DISCUSSION

In the following sections, the results of surface roughness measurements will be presented, including the quantified values of the aforementioned standard roughness metrics. Afterwards, the tensile test results of the machined and as-built specimens will be presented in terms of the effective elastic modulus, yield strength, and UTS. Finally, the results of the statistical analysis will be discussed, including the established ANOVA models.

4.1. Surface Roughness Measurement Results

The gauge sections of the fabricated thin-walled specimens were scanned with Alicona™ Infinite-Focus G5 optical device by utilizing focus variation (FV) technique. Figure 14 shows the scanned area of the up-skin and down-skin faces with the height maps of the scanned surfaces for three different specimens. As it can be observed from the Figure 14, in contrast to the up-skin surface textures, which do not significantly alter, the down-skin surface textures are sensitive to build angle. According to the study of Pegues et al., the rougher downward facing surfaces were the more critical when samples were built at an angle (Pagues, Roach, Williamson, & Shamsaei, 2018). Therefore, down-skin surface roughness values were considered to be decisive in terms of the effect of surface roughness on the tensile properties of the tested specimens.

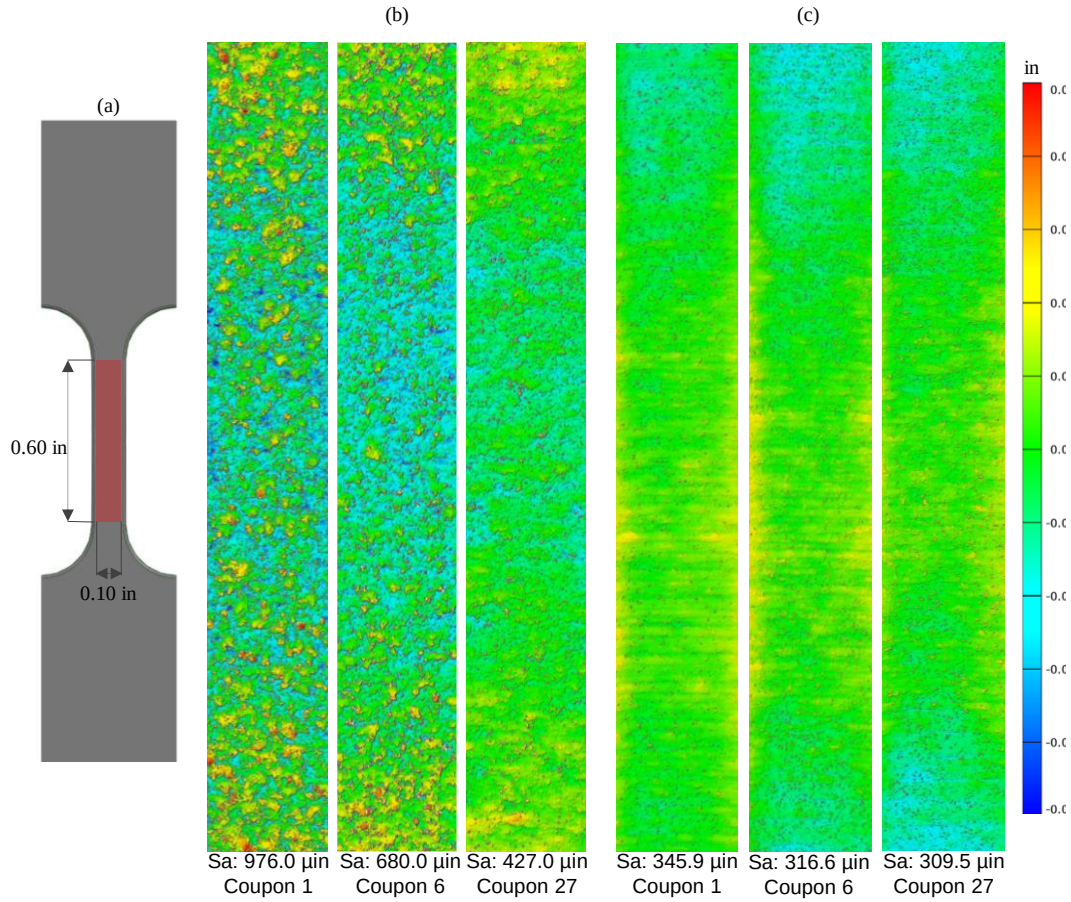

Figure 14: Height maps of the scanned surfaces a) Thin-walled coupon with the marking of the scanned area, b) Down-skin surfaces of the coupons 1, 6, and 27, c) Up-skin surfaces of the coupons 1, 6, and 27

Table 3 shows the down-skin surface roughness metrics of the thin-walled specimens. The variation of the surface roughness metrics for the specimens which have the same thickness and build angle values is due to their position with respect to the laser focal location. Sendino et al. investigated the effect of laser incidence angle on the surface roughness of the specimens produced through LPBF and concluded that the surface roughness increases as the samples are located further away from the laser focal location. In this study, the authors intentionally located the three replicate coupons on different regions of the build platform to have more variability in the resulting surface textures (Sendino, Gardon, Lartategui, Martinez, & Lamikiz, 2020).

Table 3: Down-skin surface roughness metrics of the scanned specimens

Number	Thickness (in)	Build Angle (deg)	Sa (µin)	Sq (µin)	Sp (µin)	Sv (µin)	Sz (µin)	S10z (µin)	Ssk (µin)	Sku (µin)
1	0.035	50	976	1239	5813	4466	10279	10103	0.52	3.35
2	0.035	50	786	988	5560	4626	10186	9178	0.46	3.47
3	0.035	50	1040	1329	7179	5294	12473	10975	0.56	3.57
4	0.035	60	661	839	4487	4369	8856	8662	0.41	3.68
5	0.035	60	1039	1322	6692	5011	11704	11208	0.55	3.47
6	0.035	60	680	867	5343	4036	9380	8068	0.37	3.57
7	0.035	70	326	408	2490	1313	3803	3506	0.18	3.37
8	0.035	70	411	529	2766	2498	5264	5088	0.48	3.77
9	0.035	70	594	761	4076	2886	6962	6362	0.58	3.67
10	0.055	50	1244	1583	7116	5447	12563	11870	0.67	3.47
11	0.055	50	1077	1375	7352	4926	12278	11839	0.65	3.69
12	0.055	50	911	1167	6385	4513	10898	10058	0.61	3.67
13	0.055	60	1035	1313	8485	4951	13436	10609	0.56	3.49
14	0.055	60	782	997	6818	4340	11157	10368	0.58	3.88
15	0.055	60	974	1247	6327	4759	11086	10724	0.63	3.89
16	0.055	70	525	679	4101	2727	6828	6190	0.60	4.03
17	0.055	70	628	804	4272	2772	7043	6665	0.67	3.73
19	0.075	50	1234	1571	7079	5242	12321	11750	0.68	3.49
20	0.075	50	971	1227	6252	5102	11354	10081	0.52	3.37
21	0.075	50	852	1098	5571	4241	9813	9325	0.67	3.85
22	0.075	60	796	1012	5956	4050	10006	8839	0.43	3.48
23	0.075	60	645	825	6488	3814	10302	8295	0.39	3.75
24	0.075	60	1040	1317	10328	5197	15525	11705	0.61	3.64
25	0.075	70	404	517	3732	1356	5088	4966	0.48	3.73
26	0.075	70	543	707	4635	2635	7270	6748	0.65	4.16
27	0.075	70	427	548	3351	2210	5560	5275	0.56	3.79

It should be noted that the elastic modulus is related to the crystallographic orientation of the microstructure, therefore it is not a directly thickness-dependent material property (Wan, et al., 2020). Figure 5-b shows the different regions of the cross-sections of the as-built specimens. In this figure, Tnet indicates the valley-to-valley thickness, which is expected to have the true elastic modulus of the material. However, due to the presence of unfused powder particles and surface valleys, cross-sectional area measurements by vernier calipers would overestimate the actual cross-sectional area. In addition to the reduction in material thickness, surface valleys can exhibit plastic deformation at low

strain values, which could eventually affect the slope of the stress-strain curve in the elastic region. This study evaluated the effective elastic modulus results, which can be affected by the load-carrying section variations due to the rough surfaces of the produced specimens. Caliper measurements gave values close to the nominal thickness values. Therefore, nominal cross-sectional areas of the samples were considered in the tensile testing process to build a relationship between the roughness metrics and the tensile properties.

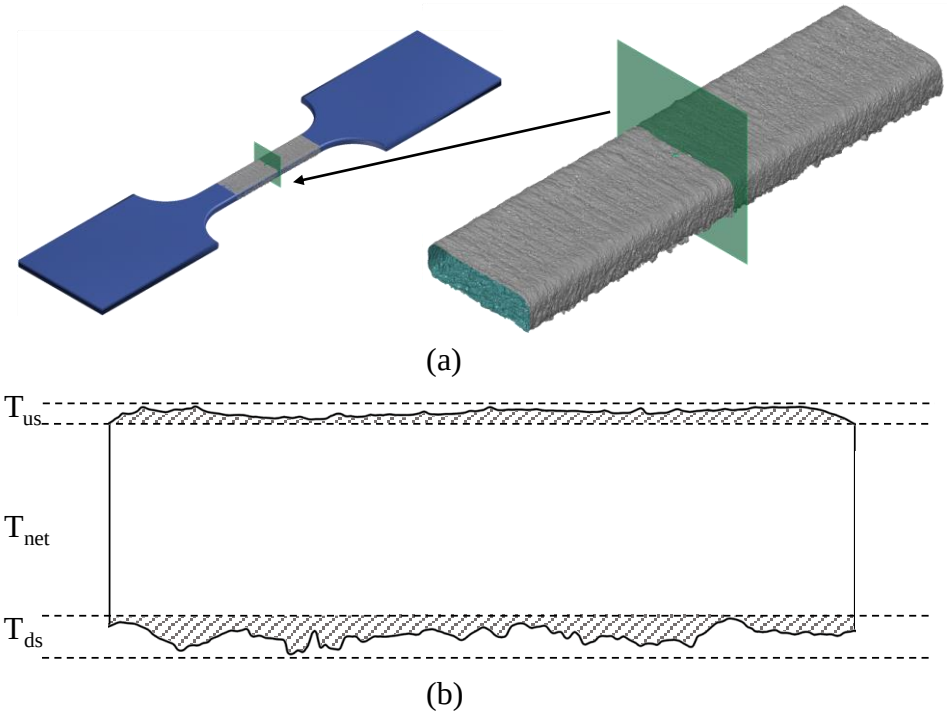

Figure 15: Cross-section characteristics of the thin-walled specimens, a) 3D scan of the gauge section, b) Schematic representation of the cross-section regions with different effective elastic modulus

4.2. Tensile Test Results

Tensile tests were performed according to ASTM E8 standard (ASTM Standard E8, 2015). Table 4 shows the tensile test results of the as-built specimens. Three replicates for each angle-thickness combination were tested. One of the specimens with 0.035 in thickness and 60 degrees build angle was eliminated due to unexpected failure. Figure 16

shows the fracture surfaces of an accepted and an eliminated specimen. It can be seen from this Figure 16-b that the specimen has an internal defect, therefore excluded from the statistical analysis procedure.

Table 4: Tensile test result of the as-built specimens

Number	Thickness (in)	Build Angle (deg)	E (msi)	Yield (ksi)	UTS (ksi)
1	0.035	50	25.7	95.3	126.4
2	0.035	50	27.7	98.5	138.5
3	0.035	50	23.4	94.3	137.2
4	0.035	60	23.2	94.3	132.4
5	0.035	60	22.5	89.2	126.2
6	0.035	60	26.5	95.1	140.8
7	0.035	70	50.9	97.3	145.5
8	0.035	70	25.1	94.6	150.3
9	0.035	70	39.3	95.5	142.6
10	0.055	50	27.7	99.1	148.8
11	0.055	50	30.0	99.4	151.2
12	0.055	50	40.9	102.3	149.7
13	0.055	60	27.5	97.8	142.4
14	0.055	60	28.0	97.4	146.5
15	0.055	60	38.2	98.6	148.1
16	0.055	70	26.8	98.1	149.1
17	0.055	70	37.5	101.4	152.4
19	0.075	50	27.6	99.2	145.0
20	0.075	50	30.8	99.1	154.9
21	0.075	50	28.9	101.9	154.4
22	0.075	60	40.0	104.2	151.0
23	0.075	60	26.7	99.8	150.5
24	0.075	60	37.5	104.8	146.6
25	0.075	70	38.6	108.2	159.1
26	0.075	70	26.0	100.8	160.8
27	0.075	70	39.1	103.5	160.8

A set of machined specimens were manufactured with varying build angles and tensile tested. Three replicates for each build angle values were tested, and the average results are given in Table 5. It is observed that the effective modulus, yield strength, and UTS were not deviated significantly with varying build angles of 50, 60 and 70 degrees.

Similar trend with varying build angles was reported by Zeng et al. (Zeng, Monu, Lupton, Lin, & Tong, 2020).

Table 5: Tensile test result of the machined specimens

Build Angle (deg)	E (Msi)	Yield (ksi)	UTS (ksi)
50	33.8	112.9	159.7
60	35.0	110.7	163.3
70	31.4	107.7	162.0
Average	33.4	110.4	161.67

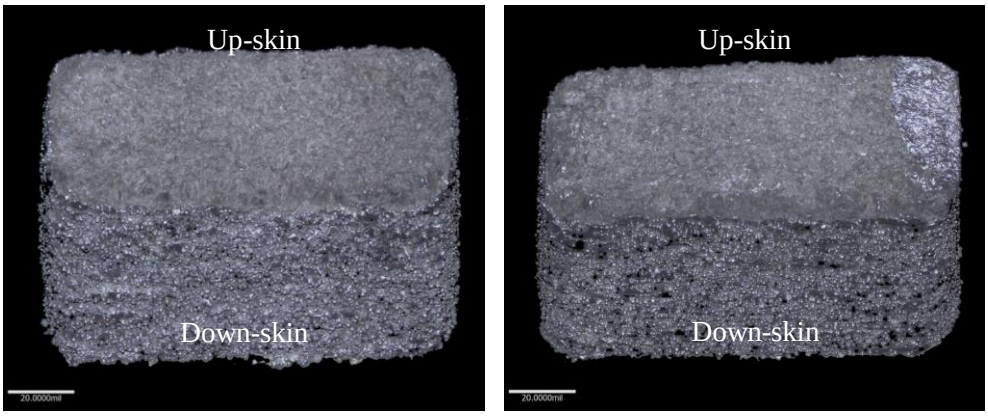

Figure 16: Fracture surfaces of the tensile tested specimens a) accepted fracture, b) rejected fracture due to an internal defect

Figure 17 shows the strain-stress plots of the as-built specimens with varying thickness values and a machined specimen. From the figure it can be observed that the stress-strain curves of the as-built samples deviates from the machined curve in different levels. This variation shows the effect of build thickness combined with the effect of surface roughness, therefore highlight the significance of these two parameters in terms of mechanical performances of the thin-walled structures produced through LPBF process. Similarly, Suh et al. demonstrated that the effect of surface roughness was more significant for the sample with lower thickness values (Suh, Jung, & Kim, 2010).

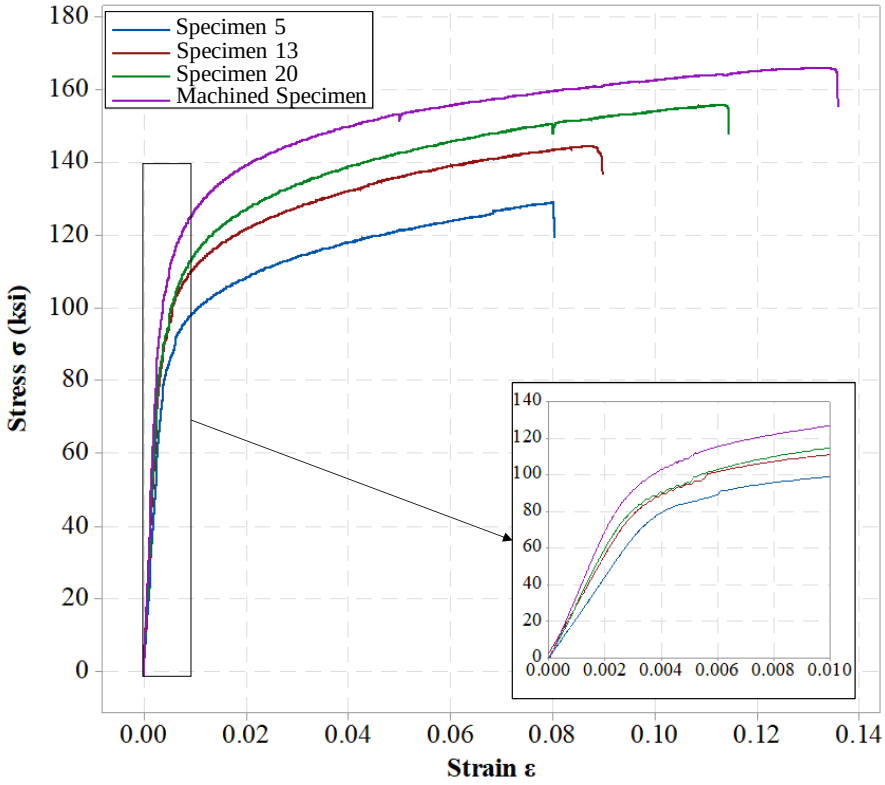

Figure 17: Strain-stress curves of specimen 5, 13, 20, and a machined sample

4.3. ANOVA

4.3.1 Effect of Design Parameters on Surface Roughness

The measured areal surface roughness results have been studied to analyse the possible influence of the build orientation, sample thickness, and angle of laser incidence on the surface quality. The sequential assessments have been carried out as defined in Section 3.4. In the regression analysis procedure, outlier data points are eliminated from the model to approach better fitted regression models. Details of the samples included into regression analysis is given in Table 6. A total of 21 data points is used in up-skin and down-skin Sa regression analyses.

Table 6: ANOVA data set for US and DS surfaces

Build orientation (degrees)	Sample thickness (in)	Distance from laser focus (in)	Sa Up-skin (µin)	Sa Down-skin (µin)
50	.035	3.381	397	1040
60	.035	5.898	367	1031
60	.035	1.505	317	680
70	.035	4.732	346	594
50	.055	5.957	410	1244
50	.055	3.270	403	1077
50	.055	3.707	369	911
60	.055	6.540	385	1035
60	.055	3.027	354	782
60	.055	5.079	385	974
70	.055	4.364	309	525
70	.055	5.502	386	628
70	.055	1.580	259	354
50	.075	6.237	380	1234
50	.075	2.977	377	971
50	.075	1.557	342	852
60	.075	4.151	336	796
60	.075	0.696	315	645
70	.075	1.903	281	404
70	.075	4.427	336	543
70	.075	3.258	325	427

The final results of the regression analysis for the down-skin and up-skin are given in the Table 7 and Table 8, respectively. The results indicate that the Sa values of the down-skin surfaces are sensitive to the O^2 and D^2 terms, while the Sa values of up-skin surfaces are sensitive to O and the interaction of O, and D terms based on the previously defined P-value criteria. The sample thickness parameter found out to be insignificant based on the same criteria.

Table 7: Regression for Sa value of down-skin surfaces

Source	DF	Adj SS	Adj MS	F-Value	P-Value
Regression	2	1408618	704309	310.04	0
$D^2(in^2)$	1	333947	333947	147.01	0
$O^2(deg^2)$	1	992587	992587	436.95	0
Error	18	40890	2272		
Total	20	1449508			

Coefficients

Term	Coef	SE Coef	T-Value	P-Value	VIF
Constant	1441.5	43.5	33.11	0	
$D^2(in^2)$	9.881	0.815	12.12	0	1
$O^2(deg^2)$	-0.2221	0.0106	-20.9	0	1

Model summary

S	R2	R2(adj)	R2(pred)
47.66	97.18%	96.87%	96.27%

With these terms a regression model is proposed for Sa as follows:

$$Sa(\mu in) = 1441.5 + 9.881\ D^2(in^2) - 0.2221\ O^2(deg^2) \quad (1)$$

where, O: Build orientation (degrees), D: Distance to laser focus (in)

Table 8: Regression for Sa value of up-skin surfaces

Source	DF	Adj SS	Adj MS	F-Value	P-Value
Regression	2	26537	13268.3	37.5	0
O(deg)	1	20066	20066.2	56.71	0
O(deg)*D(in)	1	12908	12908.4	36.48	0
Error	18	6370	353.9		
Total	20	32906			

Coefficients

Term	Coef	SE Coef	T-Value	P-Value	VIF
Constant	529.9	30.5	17.39	0	
O(deg)	-3.913	0.52	-7.53	0	1.07
O(deg)*D(in)	0.247	0.0409	6.04	0	1.07

Model summary

S	R2	R2(adj)	R2(pred)
18.8113	80.64%	78.49%	72.85%

With these terms a regression model is proposed for Sa as follows:

$$Sa(\mu in) = 529.9 - 3.913\ O(deg) + 0.2470\ O(deg)*D(in) \quad (2)$$

F-value indicates the significance level of the terms (Newton, Senin, Chatzivagiannis, Smith, & Leach, 2020). F values given in Table 7 shows that square terms of both build orientation and distance to laser focus are highly significant in terms of surface roughness of down-skin surfaces. When the F-values of the significant terms compared between up-skin and don-skin models it is observed that the significance levels of the down-skin regression terms are higher.

Table 7 and Table 8 include goodness-of-fit statistics terms S, R^2, R^2(adj), and R^2(pred). S indicates how far the data points fall from the fitted values and it is measured in the unit of the response (µin). In general, lower S value means that the model represents the response better (Newton, Senin, Chatzivagiannis, Smith, & Leach, Feature-based characterisation of Ti6Al4V electron beam powder bed fusion surfaces fabricated at different surface orientations, 2020).

R^2 and R^2 adjusted values of the regression models for down-skin and up-skin surfaces are used for observing the current status of the established regression model. For down-skin regression model, R^2 value of 97.18% implies that the resultant regression model can explain 97.18% of the variation in the response. High R^2 value means that the model fits well with the data. In general, R^2 value increases as new terms added to the regression model. Therefore, R^2 adjusted is a more convenient criteria to understand if addition of a new term results in more reliable regression model (Ghorbani, Li, & Srivastava, Application of optimized laser surface re-melting process on selective laser melted 316L stainless steel inclined parts, 2020). R^2 adjusted values are used to compare the models with different number of predictors as the insignificant terms are eliminated step-by step. The results showed that the proposed regression model reflects the variability in up-skin Sa values by an adjusted R^2 value of 78.49%.

The predicted R^2 indicates that how well the final regression model fits the response for new observations. Models with high predicted R^2 values represents better fitting for the new observed data (Newton, Senin, Chatzivagiannis, Smith, & Leach, Feature-based characterisation of Ti6Al4V electron beam powder bed fusion surfaces fabricated at

different surface orientations, 2020). For the final down-skin regression, R^2 predicted value of 96.27% indicates fitness of the proposed prediction model (Table 7). Considering the R^2 predicted value of 72.85% for the up-skin regression (Table 8), the level of fitness for the up-skin regression model is less than the regression model for the down-skin surfaces.

The reason for the lower R^2 predicted and R^2 adjusted values for up-skin Sa regression model could be the lower significance level of the build orientation and distance from laser focus parameters when the F values compared with the down-skin Sa regression model. The presence of overhangs for down-skin faces makes the build angle parameter highly significant for down-skin surface roughness. Due to overhangs, the effect of laser incidence angle also varies between up-skin and down-skin faces (Kleszczynski, et al., 2015).

After determining the significant factors with ANOVA for up-skin and down-skin Sa values, the influencing parameters are presented individually to show the trends for each parameter. As it is concluded from Table 7 and Table 8, the Sa values of both down-skin and up-skin surfaces are thoroughly a function of the build angle and distance from laser focus. Figure 18 shows the effects of the build angle on the down-skin and up-skin surface roughness, respectively. As it can be observed, higher surface roughness is measured for specimens located with lower build angle with respect to the build platform. The results showed that the surface roughness is dependent on the build orientation of the specimens for both down-skin and up-skin surfaces. A similar trend was also reported in (Tian, Tomus, Rometsch, & Wu, 2017).

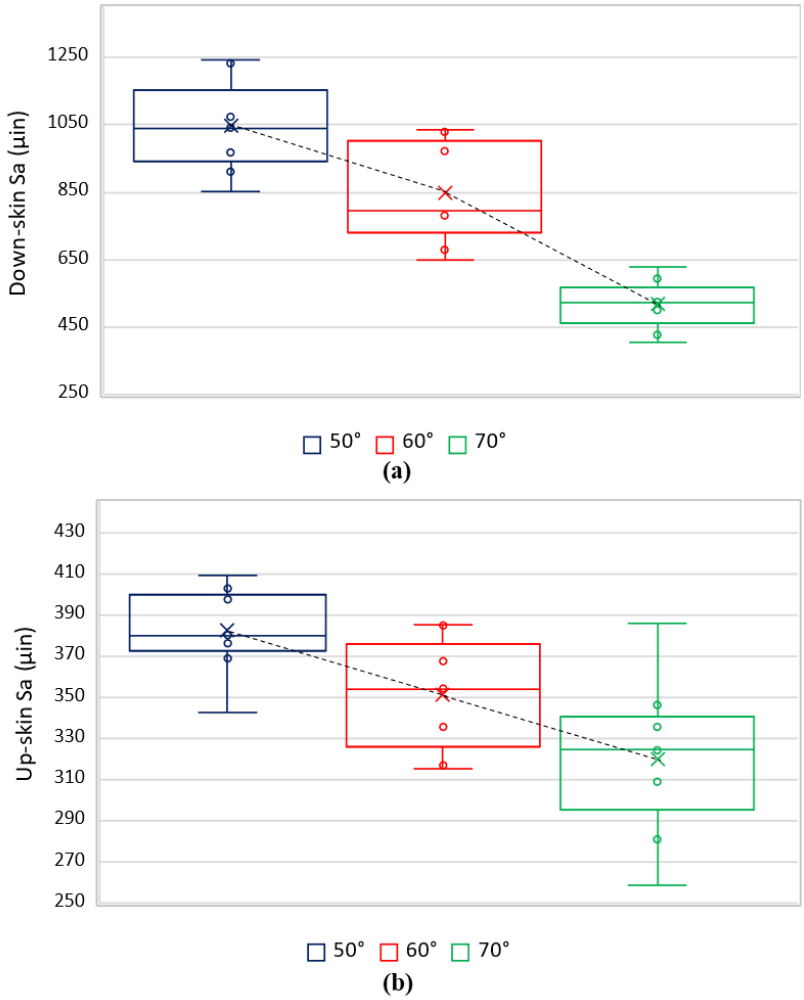

Figure 18: Surface roughness of selective laser melted samples with various degrees of build angle (a)Down-skin surfaces, (b)Up-skin surfaces

Another characterization was carried out to understand the variation of the surface roughness with varying angle of the laser incidence. For this purpose, instead of actual laser incidence angle, the measured distances between the projected location of the laser on the build platform and the mid-points of the gauge sections are taken into consideration for each sample.

Figure 19 shows the effect of distance to laser focal location, thereby the effect of the angle of incidence, on the surface roughness of down-skin and up-skin surfaces. The results show that even though the specimens were manufactured using the same thickness, build angle and process parameters, the surface roughness is influenced by the position of the specimen on the build plate. As it can be observed in Figure 19, a higher surface roughness is measured for the specimens located away from the laser. More specifically, for the specimens oriented at 50°, the down-skin surface roughness increases

from values of Sa = 851.9 µin for the specimen closest to the laser to Sa = 1244.0 µin for the specimen at the farthest. Similar trends can be observed for the other specimens manufactured with different build orientations (Sendino, et al., 2020).

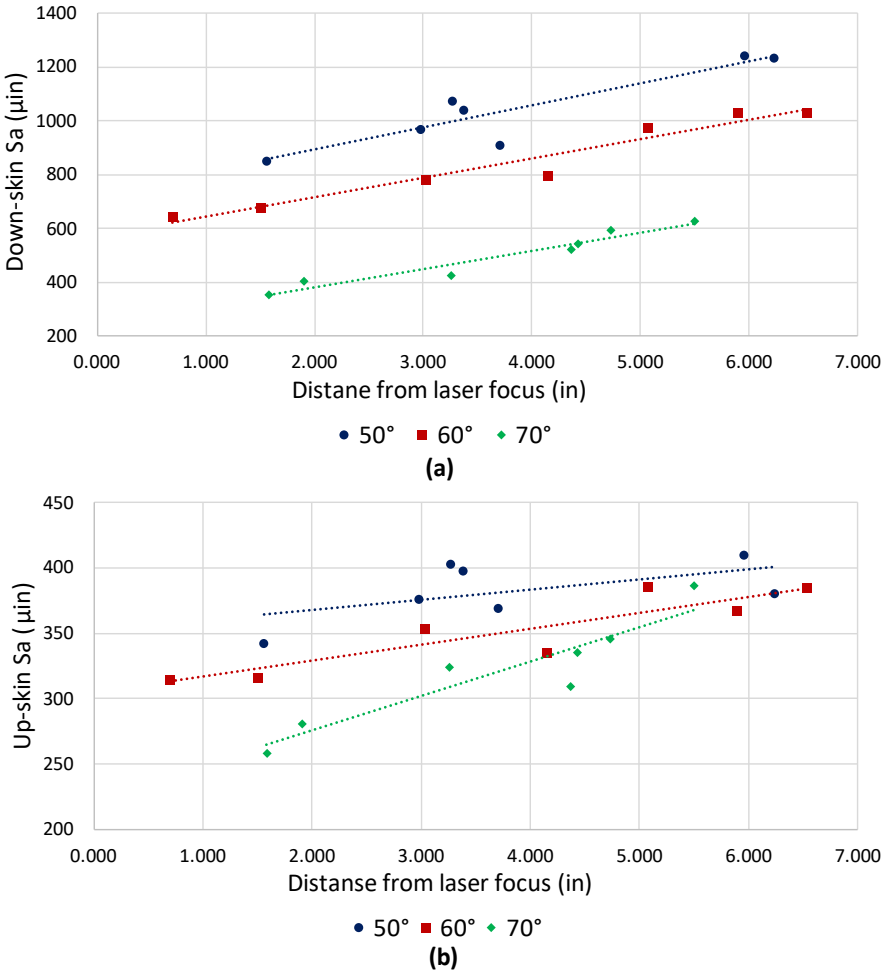

Figure 19: Surface roughness of selective laser melted samples with various distances from laser focus (a)Down-skin surfaces, (b)Up-skin surfaces

Due to variation in the angle of laser incidence, the shape of the laser spot gets a non-circular shape at the areas further away from the laser focal location. Consequently, the powder bed is heated differently from the laser focus area and melt pool is not formed in the same way (Kleszczynski, et al., 2015). The effect of this variation is found to be more significant for the down-skin surfaces compared to the up-skin surfaces. For the down-skin surfaces, instabilities at the melt pool regions are suspected to occur due to combination of overhangs and laser incidence angle. These instabilities could cause melt extensions and un-melted particles to stick on the surface (Kleszczynski, et al.,

2015). Figure 20 shows a representation of the incidence angle situation for down-skin and up-skin surfaces.

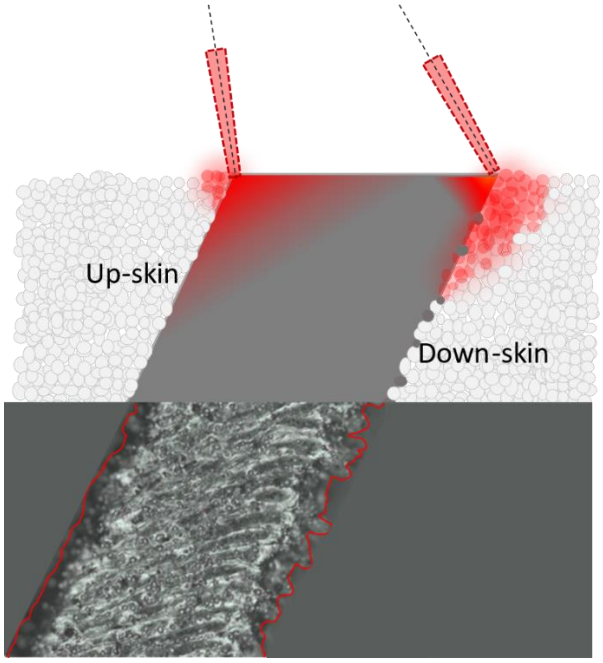

Figure 20: Enlarged schematic representation for up-skin and down-skin surfaces *(Kleszczynski, et al., 2015)*

4.3.2 Effects of Sample Thickness and Surface Roughness on Tensile Properties

In this section, the correlation between the surface roughness metrics and tensile properties was discussed. A Pearson correlation test was conducted to identify the most significant roughness metrics for each tensile property (Pearson, 1909). The Pearson correlation coefficients (PCC) and the P-values of each variable are reported in Table 9. One noteworthy observation from the processing of the Pearson correlation test was that there is a strong correlation between the sample thickness and yield strength, and UTS. Thickness dependency for effective elastic modulus was also observed in trend plots and the ANOVA process. Based on the results of the Pearson test, Sv and S10z was found to be correlated with effective elastic modulus while Sa and Sq was also found to be related in the ANOVA analysis. Although Sz parameter has P value slightly higher than 0.05, this this parameter was eliminated in the sequential ANOVA assessments for converging the highest possible model reliability. Pearson test also revealed that Sv and Sku is

correlated with UTS based on the P-value criteria. In the ANOVA process S10z was also be found to be correlated with UTS. ANOVA results will be presented in the following sections. Additionally, it was found that there is a direct relationship between the yield strength and the sample thickness. However, a direct influence of surface roughness metrics on the yield strength was not identified from the processed data.

Table 9: Pearson correlation map for surface roughness metrics and tensile properties

		Sa	Sq	Sp	Sv	Sz	S10z	Ssk	Sku
E	PCC	-0.341	-0.345	-0.26	-0.472	-0.36	-0.411	-0.233	-0.086
	P-value	0.088	0.085	0.199	0.015	0.071	0.037	0.252	0.678
Yield	PCC	-0.150	-0.149	0.047	-0.267	-0.084	-0.159	0.188	0.241
	P-value	0.463	0.468	0.818	0.188	0.683	0.437	0.358	0.236
UTS	PCC	-0.354	-0.347	-0.233	-0.442	-0.331	-0.373	0.234	0.523
	P-value	0.076	0.082	0.252	0.024	0.100	0.061	0.251	0.006

Average effective elastic modulus, yield strength, and UTS values for varying thicknesses of as-built specimens are plotted in Figure 21 with markings of reference machined specimen average values. It is observed that the as-built samples with 0.035 in thickness shows the highest debits for all the listed mechanical properties. Regardless of the sample thickness, all as-build specimens have lower average effective elastic modulus, yield strength, and UTS compared to the machined specimen while the difference increases as the specimens get thinner. Highest reduction in tensile properties were observed for the samples with 0.035 in thickness. When the average effective elastic modulus values considered, the amount of reduction is around 12% compared to the machined samples. In addition to the effect of surface roughness, geometric variations which could not be captured with caliper measurements, existence of internal defects and localized plastic deformations along the rough surfaces could contribute to such a high difference. Overall, it is observed that, for the as-built samples, tensile properties improved as the sample thickness increased. Similar result was also reported in the study performed by Algardha et al. As the sample thickness increases, bulk properties of the samples become dominant and capable of overcoming the effect of rough surfaces (Algardh, et al., 2016).

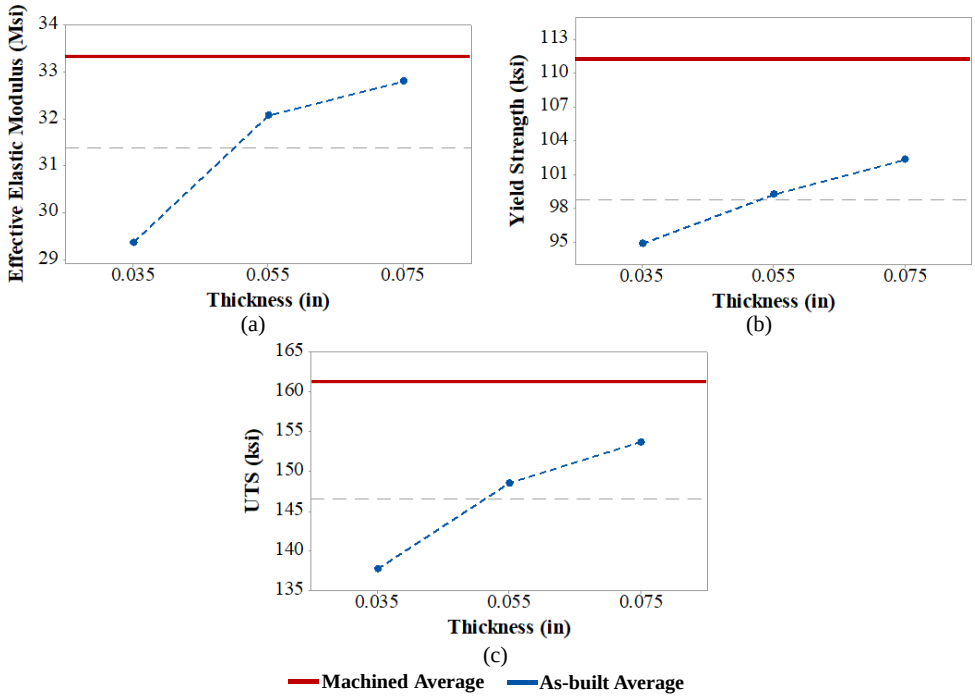

Figure 21: Average values of the tensile test results with thickness categorization a) Effective elastic modulus, b) Yield strength, and c) UTS

Figure 22 and Figure 23 shows the trend plots for the most significant surface roughness parameters in terms of effective elastic modulus and UTS values of the samples with 0.035-in thickness. Similar trends were observed for the samples with 0.055- and 0.075-in thickness with the trend for 0.035-in thick samples was more visible.

The main reason of the lower mechanical properties for the unfinished surfaces was addressed by Everhart et al. as the reduction in the cross-sectional area due to existence of the surface roughness (Everhart, Sawyer, Neidt, Dinardo, & Brown, 2016). Based on this finding, effect of Sv on the effective elastic modulus could be explained since the surface valleys are the main contributors to lower load carrying cross-sections. Similarly, Sa, Sq, and S10z parameters includes the effect of surface valleys therefore could be responsible for effective elastic modulus reduction. Sv values were also reported to be significant for fatigue life in several research (Gockel, Sheridan, Koerper, & Whip, 2019) (Lee, Rasoolian, Silva, Pegue, & Shamsei, 2021). When Sv values are considered, the reduction in UTS is likely caused by the early crack initiation rates cause by the driving forces occurred due to increased magnitude and number of surface valleys (Watring, Carter, Crouse, Raeymaekers, & Spear, 2019).

In the study of Lee et al, it was suggested to use skewness and kurtosis parameters together to better evaluate the surface texture distribution (Lee, Rasoolian, Silva, Pegue, & Shamsei, 2021). For our study, skewness was not found to be correlated with the varying build parameters therefore there were not significant differences between the generated surface textures in terms of Ssk values. Kurtosis parameter is a quantification of the sharpness of the distribution of the surface texture. A Sku value of three, indicates a normal distribution. The surface height distribution becomes spiked when the Sku is greater than three and becomes flat when Sku is less than three (Lee, Rasoolian, Silva, Pegue, & Shamsei, 2021). Figure 3 can be referred for better clarification of the skewness and kurtosis parameters by considering a 2D surface texture.

In this study, all skewness values were greater than zero which indicates that there is a predominance of peaks in the surface distribution. Kurtosis explains the distribution sharpness and highlights whether the peaks and valleys of the surface profile are either steep or rounded (Duboust, et al., 2016). Based on this explanation, surfaces with high kurtosis values can have round transitions between peaks and valleys which could reduce the local stress concentrations. This could eventually affect UTS positively by reducing the local plastic deformations.

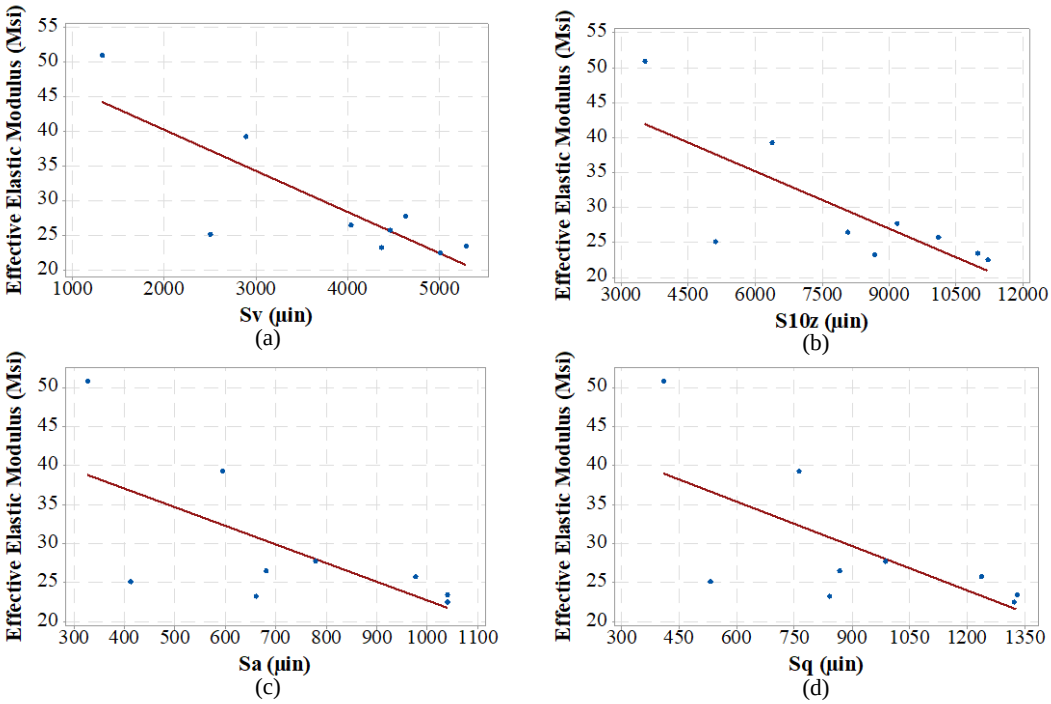

Figure 22: Significant surface roughness metrics – Effective elastic modulus for the samples with 0.035 in thickness a) Sv - Eff. Elastic Modulus, b) S10z - Eff. Elastic Modulus, c) Sa - Eff. Elastic Modulus, and d) Sq - Eff. Elastic Modulus

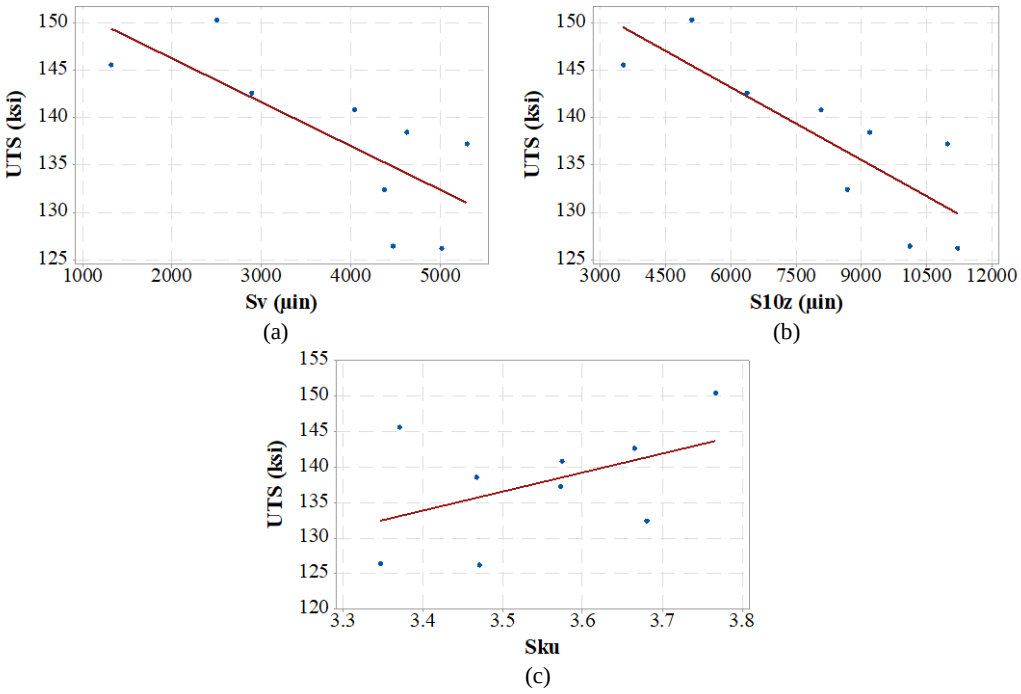

Figure 23: Significant surface roughness metrics – UTS for the samples with 0.035 in thickness a) Sv - UTS, b) S10z - UTS, and c) Sku – UTS

Based on the Pearson correlation test results, a sequential regression analysis process has been carried out as described in the previous chapter. The regression analyses were

performed with a total of 26 data points. A reliable regression model could not be established for yield strength with the current data set therefore any further assessments were not addressed in the following sections. ANOVA results and the regression models for effective elastic modulus and UTS were discussed in the next sections.

4.3.2.1. Elastic modulus vs input variables

It was found that the effective elastic modulus of the printed as-built specimens is related to the Sv and S10z. When comparing the thickness and surface roughness metrics to the elastic modulus, the elastic modulus increases with an increasing sample thickness while surface roughness metrics are inversely correlated to the elastic modulus. This emphasizes the need for a proper sample thickness and process parameter set to improve the surface quality for an optimal effective elastic modulus.

In addition to aforementioned variables that have a significant impact on the effective elastic modulus, Sa and Sq was also included into the regression model while the P-value of it was slightly higher than 0.05, according to the Pearson correlation map. This enabled to cover the second order term and the interaction effects and improved the key parameters, R^2, R^2 adjusted, and R^2 predicted, of the regression model. The finalized ANOVA and regression results are provided in Table 10.

In the ANOVA table, F-values measures the significance level of the terms and higher F-values point out that the corresponding term has a significant impact on the output variable (Montgomery, 2017). The ANOVA results for the elastic modulus reveals that the interaction term of Sa and thickness is the most significant term when the F-values are compared. Other than the thickness terms, the most effective term is the square term of Sv parameter. The reliability of the established regression models can be tested by evaluating the goodness of the fit terms S, R^2, R^2(adj), and R^2(pred). The S value quantifies the difference between fitted values and actual data points, and it has the unit of the response. In general, lover S-values indicate that there is a good agreement between regression models and the used data points (Montgomery, 2017). The S value given in

the Table 10 is 3.53 for the effective elastic modulus, which indicates the regression model is sufficient for further assessments. The R^2 is an indicator to quantify how accurate the data fits to the established regression model. In general, higher values of R^2 denote that the data fits well with the model (Ghorbani, Li, & Srivastava, 2020). The R^2 value of 86.57% for the elastic modulus indicates that the model explains 86.57% of the variation in the response. On the other hand, the R^2(adj) defines the percentage of variation explained by only the variables that affect the response variable. Therefore, R^2(adj) is a more suitable criterion to evaluate if the addition of the new terms results in a well fitted model (Ghorbani, Li, & Srivastava, 2020). R^2(adj)values were utilized to make comparisons between the regression models with varying number of predictors as the insignificant terms were eliminated in the subsequent iterations. The calculated R^2(adj) value is 76.02% for the elastic modulus.

Table 10: ANOVA and regression results for elastic modulus

Analysis of Variance					
Source	DF	Adj SS	Adj MS	F-Value	P-Value
Sa (µin)	1.00	55.74	55.74	4.50	0.05
Sv (µin)	1.00	118.71	118.71	9.57	0.01
Sa (µin)* Sa (µin)	1.00	158.64	158.64	12.79	0.00
Sv (µin) * Sv (µin)	1.00	218.62	218.62	17.63	0.00
S10z (µin) * S10z (µin)	1.00	157.41	157.41	12.69	0.00
T (in)* Sa (µin)	1.00	255.09	255.09	20.57	0.00
T (in)* Sq (µin)	1.00	252.81	252.81	20.39	0.00
Sa (µin)*Sq (µin)	1.00	158.12	158.12	12.75	0.00
Sa (µin)*Sv	1.00	118.25	118.25	9.54	0.01
Sq (µin)*Sv (µin)	1.00	122.85	122.85	9.91	0.01
Sv (µin)*S10z (µin)	1.00	160.77	160.77	12.97	0.00
Error	14.00	173.59	12.40		
Total	25.00	1292.81			
Model Summary					
S	R-sq		R-sq(adj)	R-sq(pred)	
3.53	86.57%		76.02%	60.07%	

4.3.2.2. UTS vs input variables

The most significant roughness metrics for the UTS were determined to be Sv, S10z, and Sku. The specimen thickness and UTS are positively correlated, while an increase in the value of the roughness metrics has a negative impact on UTS. All significant variables were employed in ANOVA process to establish regression models.

The results of the ANOVA were given in the Table 11. The predefined key regression parameters, S, R^2, R^2(adj), and R^2(pred) were 3.67, 88.29%, 83.73%, and 77.18%, respectively. These results confirm that the regression model can capture the actual data points accurately, however as with the effective elastic modulus regression model, a larger data set can be beneficial to improve the predictive capability of the regression model.

Table 11: ANOVA and regression results for UTS

Analysis of Variance					
Source	DF	Adj SS	Adj MS	F-Value	P-Value
T(in)	1.00	163.31	163.31	12.15	0.00
Sv(µin)	1.00	74.75	74.75	5.56	0.03
S10z(µin)	1.00	101.39	101.39	7.54	0.01
T(in)*T(in)	1.00	104.72	104.72	7.79	0.01
S10z(µin)* S10z(µin)	1.00	86.2	86.20	6.41	0.02
Sv(µin)*Sku	1.00	67.68	67.68	5.04	0.04
S10z(µin)*Sku	1.00	77.14	77.14	5.74	0.03
Error	18.00	241.9	13.44		
Total	25.00	2064.87			

Model Summary			
S	R-sq	R-sq(adj)	R-sq(pred)
3.67	88.29%	83.73%	77.18%

4.4. Finite Element Analysis

For the validation of the trend observed for the thickness dependency on the effective elastic modulus, finite element models were created in varying thickness values with same surface topology. To achieve a rough surface, a Python code was introduced to have a randomized point cloud accounting for desired maximum, minimum and average values of the distribution. Randomized point cloud then used for forming a surface in Rhino™ software and the surface was extruded in different values taking the mean plane as reference to have volumes which have varying thickness values. Models were subjected to 1% tensile strain in ANSYS™ to simulate the tensile test conditions. Reaction forces taken from the strain applied faces were utilized to calculate effective elastic modulus values using equation 1.

$$Eeff = \frac{F}{A * \varepsilon} \tag{3}$$

where,

E_{eff}: Effective elastic modulus, F: Reaction force, A: Cross-sectional area, and ε: Tensile strain

Cross sectional area was calculated by using the mean plane of the surfaces. Figure 24 shows the employed boundary conditions with the equivalent stress results for the 0.015-in thick model. Tensile strain was applied from Y faces while the bottom Z and X faces were fixed in the normal directions. Average machined specimen mechanical properties were used in the analyses of the 0.060 x 0.060 sized sections. As it can be observed from the figure, peaks of the surface do not carry load while the maximum stresses occur at the valleys.

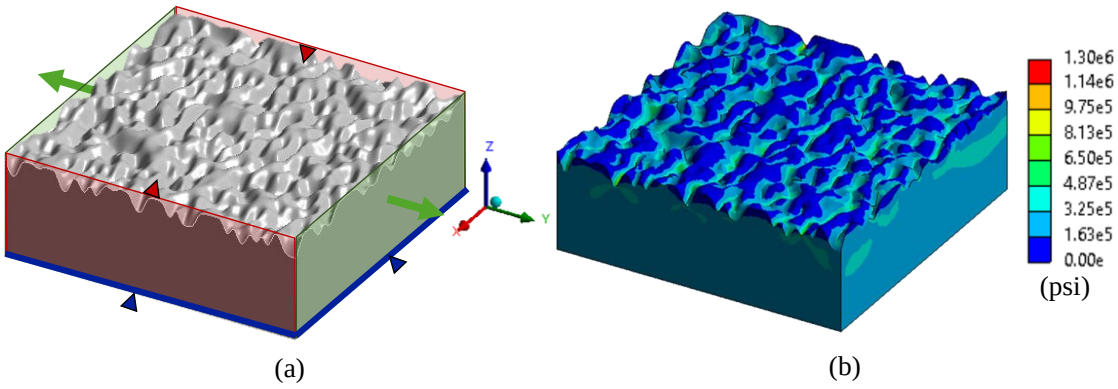

(a) (b)

Figure 24: Finite element model for rough surfaces, a) Boundary conditions, b) Equivalent stress color plot for the model with 0.015-in thickness

The analyses were performed for various thickness values from 0.015-in to 0.075-in with 0.010-in increment to observe the change in effective elastic modulus for the cases with the same surface topology and different thickness values. Figure 25 shows the results of the effective elastic modulus values for the cases with varying thicknesses with the marking of the result of a case without roughness with the red line. Results of the performed analyses showed that the effect of surface roughness on the mechanical performance decreases as the samples gets thicker. Similar conclusion was made according to the experimental results. Other studies have also reported the thickness dependency of the mechanical properties (Algardh, et al., 2016) (Suh, Jung, & Kim, 2010). However, the magnitudes of the effective elastic modulus could not be matched with the experimental results. The main reason for this could be that the performed analyses do not account for the local plastic behavior which could occur during tensile loading. On the other hand, existence of internal gaps was not captured by the finite element models which could be another reason for overestimating the effective elastic modulus compared to the experimental results. To achieve a more realistic representation of the experimental results, surface models can be modified to reflect the distribution of the real surfaces and the plastic material properties can be introduced to the models.

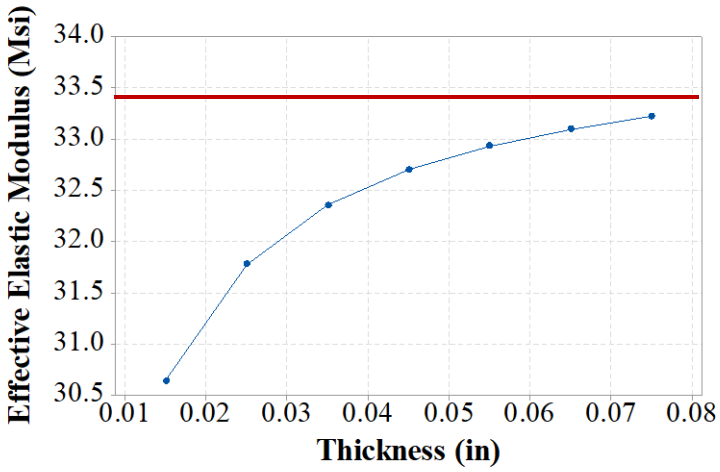

Figure 25: Change in effective elastic modulus with varying thickness values for the FEA models

5. CONCLUSION AND FUTURE WORKS

This study provides an experimental procedure and a statistical analysis to reveal the most influential surface roughness metrics on the tensile properties of CoCr thin-walled samples produced through LPBF process. This work also investigates the effects of the build angle, build thickness, and laser incidence angle on surface roughness of additively manufactured thin-walled CoCr specimens. Laser incidence angle was controlled by varying the sample location on the build platform with respect to laser origin. The findings from the present study are listed below:

1. For up-skin and down-skin surface roughness, the impact of the build angle and the sample location with respect to projected location of the laser onto build platform was found to be significant.
2. It is concluded that the surface roughness increases as the samples were positioned away from the laser origin or as the laser incidence angle increases.
3. The significance level of the distance to laser focus parameter was found to be lower for up-skin Sa compared to down-skin Sa. For down-skin surfaces, instabilities at the melt pool could cause melt extensions and un-melted particles to stick on the surface due to a combination of overhangs and laser incidence angle.
4. The surface roughness of the up-skin and down-skin surfaces depends on the build angle. Surface roughness increases as the build angle with respect to build platform decreases.
5. According to ANOVA results, the sample thickness was found to be insignificant in terms of surface roughness. However, there are studies that reported the significance of sample thickness in terms of surface roughness. For

this study, the thickness interval was limited, and the other factors were more dominant. Therefore, a significance for sample thickness was not observed.

6. The tensile test results showed that the effective elastic modulus, yield strength and the UTS values of the as-built samples were lower than the machined specimens.
7. The negative effect of surface roughness on the effective elastic modulus, yield strength, and UTS values reduces when the sample thickness increases.
8. According to the results of the Pearson correlation test, yield strength could only be related to sample thickness while no surface roughness metric could be found to be more significant than the others.
9. Statistical analysis procedure revealed that Sa, Sq, Sv, and S10z parameters are more significant in terms of effective elastic modulus compared to the other surface roughness metrics.
10. For UTS values, statistical analysis revealed that Sv, S10z, and Sku parameters were more significant compared to the other surface roughness metrics.

Overall results indicate that the sample position on the build platform could be an important build planning parameter in terms of surface quality of the end-products with the consideration of the laser incidence angle. Build orientation of the thin-walled samples should also be considered for having as-built surfaces with less roughness for the critical applications. While designing thin-walled structures, effect of surface roughness should be assessed in terms of its effects on the mechanical performance. It could be beneficial to perform trade-off studies between having a light-weighted components with thin-walled structures and the reduction of the mechanical performance due to existence of the as-built surfaces.

The effects of design parameters on surface roughness were demonstrated in this study. The effects of other build parameters such as laser power, scan speed, and hatch distance can be investigated in terms of their effects on the areal surface roughness metrics. Build and design parameters can be optimized to determine surface roughness metrics and to improve desired mechanical properties of the end product.

The influence of surface texture on the mechanical performance of thin-walled structures can be further investigated with additional hybrid surface roughness metrics. New formulations can be developed by combining the standard surface metrics to better

explain the effect on mechanical properties. The shapes and sizes of the surface features can be investigated in terms of their effects on material failure through additional fractographic inspections. The surface roughness metrics can also be examined in terms of their effects on the effective cross-sectional area of the produced samples. These investigations can provide a better understanding of the significance of roughness metrics on mechanical behaviour. Similar studies can also be performed for different metallic alloys to investigate material-dependent effects of surface roughness metrics.

To reduce time and cost efficiency, modelling techniques can be developed to mimic fabricated surface textures. In addition to maximum, minimum, and average values, surface metrics that reflect the shape of the surface height distribution can be used to create more realistic surface textures. These created surface textures can be analysed through FEA with elastic-plastic material properties to account for local plastic behaviour along the surface texture.

BIBLIOGRAPHY

Algardh, J. K., Horn, T., West, H., Aman, R., Snis, A., Engqvist, H., . . . Harrysson, O. (2016). Thickness dependency of mechanical properties for thin-walled titanium parts manufactured by Electron Beam Melting (EBM)®. *Additive Manufacturing, 12*, 45-50. doi:10.1016/j.addma.2016.06.009

Arola, D., & Ramulu, M. (1999). An Examination of the Effects from Surface Texture on the Strength of Fiber Reinforced Plastics. *Journal of Composite Materials, 33*(2), 102-123. doi:10.1177/002199839903300201

ASTM Standard E8. (2015). *Standard test methods for tension testing of metallic materials.* West Conshohocken: ASTM International.

Blakey-Milner, B., Grandl, P., Snedden, G., Brooks, M., Pitot, J., Lopez, E., . . . du Plesis, A. (2021). Metal additive manufacturing in aerospace: A review. *Materials & Design, 209*, 110008.

Chakraborty, A., Tangestani, R., Batmaz, R., Muhammad, W., Plamondon, P., Wessman, A., . . . Martin, E. (2022). In-process failure analysis of thin-wall structures made by laser powder bed fusion additive manufacturing. *Journal of Materials Science & Technology, 98*, 233–243.

Charles, A., Elkaseer, A., Thijs, L., Hagenmeyer, V., & Scholz, S. (2019). Effect of process parameters on the generated surface roughness of down-facing surfaces in selective laser melting. *Applied Sciences, 9*(6), 1256.

Covarrubias, E. E., & Eshraghi, M. (2018). Effect of build angle on surface properties of nickel superalloys processed by selective laser melting. *JOM, 70*(3), 336–342. doi:10.1007/s11837-017-2706-y

DebRoy, T., Wei, H. L., Zuback, J. S., Mukherjee, T., Elmer J, W., Milewski, J. O., . . . Zhang, W. (2018). Additive manufacturing of metallic components – Process, structure and properties. *Progress in Materials Science, 92*.

Direct metal laser melting. (2022). Retrieved from GE Additive: https://www.ge.com/additive/direct-metal-laser-melting

Duboust, N., Ghadbeigi, H., Pinna, C., Ayvar-Soberanis, S., Collis, A., Scaife, R., & Kerrigan, K. (2016). An optical method for measuring surface roughness of machined Carbon Fibre Reinforced Plastic composites. *Journal of Composite Materials, 51*(3), 289-302. doi:10.1177/0021998316644849

Eidt, W., Tatman, E. P., McCarther, J., Kastner, J., Gunther, S., & Gockel, J. (2019). Surface roughness characterization in laser powder bed fusion additive manufacturing. *International Solid Freeform Fabrication Symposium.* Austin: University of Texas.

Emmelman, C., Kranz, J., Herzog, D., & Wycisk, E. (2016). Laser additive manufacturing of metals. In V. Schmidt, & M. R. Belegratis, *Laser Technology in Biomimetics Basics and Applications* (pp. 371-392). Berlin: Springer.

EN ISO 11562. (1996). *Geometrical product specifications- surface texture: Profile method- metrological characteristic of phase corects filters.*

Everhart, W., Sawyer, E., Neidt, T., Dinardo, J., & Brown, B. (2016). The effect of surface finish on tensile behavior of additively manufactured tensile bars. *Materials Science, 51*(8), 3836–3845.

Frazier, W. E. (2014). Metal Additive Manufacturing: A Review. *Journal of Materials Engineering and Performance, 23*(6), 1917-1928.

Gathimba, N., & Kitane, Y. (2021). Effect of surface roughness on tensile ductility of artificially corroded steel plates. *Journal of Constructional Steel Research, 176*. doi:10.1016/j.jcsr.2020.106392

Ghidossi, P., El Mansori, M., & Pierron, F. (2004). Edge machining effects on the failure of polymer matrix composite coupons. *Composites Part A: Applied Science and Manufacturing, 35*(7-8), 989–999. doi:10.1016/j.compositesa.2004.01

Ghorbani, J., Li, J., & Srivastava, A. K. (2020). Application of optimized laser surface re-melting process on selective laser melted 316L stainless steel inclined parts. *Journal of Manufacturing Processes, 56*, 726-734.

Gockel, J., Sheridan, L., Koerper, B., & Whip, B. (2019). The influence of additive manufacturing processing parameters on surface roughness and fatigue life. *International Journal of Fatigue, 124*, 380-388.

Gülcan, O., Simsek, U., Cokgunlu, O., Özdemir, M., Şendur, P., & Yapici, G. G. (2022). Effect of build parameters on the compressive behavior of additive manufactured CoCrMo lattice parts based on experimental design. *Metals, 12*(7), 1104.

Herring, M. L., Mardel, J. I., & Fox, B. L. (2010). The effect of material selections and manufacturing process on the surfce finish of carbon-fibre composites. *Journal of Material Pocess Technologies, 210*, 926-940.

Herzog, D., Seyda, V., Wycisk, E., & Emmelmann, C. (2016). Additive manufacturing of metals. *Acta Materialia, 117*, 371-392.

Hossain, U., Ghouse, S., Nai, K., & Jeffers, J. R. (2021). Mechanical and morphological properties of additively manufactured SS316L and Ti6Al4V micro-struts as a function of build angle. *Additive Manufacturing, 46*.

ISO 25178-2. (2012). *Geometrical product specifications (GPS) – surface texture: Areal- Part 2: Terms, definitions and surface texture parameters.*

ISO 4287. (2000). *Geometrical product specification (GPS) Surface texture: Profile method Terms, definitions and surface texture parameters.* British Standards Institute.

ISO/ASTM 52900. (2021). *Additive manufacturing general principles fundamentals and vocabulary.* Geneva, Switzerland and West Conshohocken, PA, USA.

Kleszczynski, S., Ladewig, A., Frienberger, K., Zur Jacobsmühlen, J., Merhof, D., & Witt, G. (2015). Position dependency of surface roughness in parts from laser beam melting systems. *International Solid Freeform Fabrication Symposium.* Austin: University of Texas.

Konieczny, B., Szczesio-Wlodarczyk, A., Sokolowski, J., & Bociong, K. (2020). Challenges of Co–Cr alloy additive manufacturing methods in dentistry—The current state of knowledge (systematic review). *Materials, 13*(16), 3524. doi:10.3390/ma13163524

Kotzem, D., Dumke, P., Sepehri, P., Tenkamp, J., & Walther, F. (2020). Effect of miniaturization and surface roughness on the mechanical properties of the electron beam melted superalloy Inconel®718. *Progress in Additive Manufacturing*, 267–276.

Lebea, L., Ngwangwa, H. M., Desai, D., & Nemavhola, F. (2021). Experimental investigation into the effect of surface roughness and mechanical properties of 3D-printed titanium Ti-64 ELI after heat treatment. *International Journal of Mechanical and Materials Engineering, 16*(1). doi:10.1186/s40712-021-00138-2

Lee, S., Rasoolian, B., Silva, D. F., Pegue, J. W., & Shamsei, N. (2021). Surface roughness parameter and modeling for fatigue behavior of additive manufactured parts: A non-destructive data-driven approach. *Additive Manufacturing, 46*. doi:10.1016/j.addma.2021.102094

Lu, X., Chiumenti, M., Cervera, M., Tan, H., Lin, X., & Wang, S. (2021). Warpage analysis and control of thin-walled structures manufactured by laser powder bed fusion. *Metals, 11*(5), 686.

Memu, F., Hamat, B. A., Güleç, Y., & Durlu, N. (2019). Effect of Surface Roughness on Tensile Properties of Electron Beam Melted Ti-6Al-4V Alloy. *Euro PM 2019 Congress and Exhibition.* European Powder Metallurgy Association (EPMA).

Montgomery, D. C. (2017). *Design and analysis of experiments.* John Wiley & Sons.

Newton, L., Senin, N., Chatzivagiannis, E., Smith, B., & Leach, R. (2020). Feature-based characterisation of Ti6Al4V electron beam powder bed fusion surfaces fabricated at different surface orientations. *Additive Manufacturing, 35*. doi:10.1016/j.addma.2020.101273

Obilanade, D., Dordlofva, C., & Törlind, P. (2021). Surface Roughness Considerations in Design for Additive Manufacturing - A Literature Review. *Proceedings of the Design Society, 1*, 2841-2850. doi:10.1017/pds.2021.545

Pagues, J., Roach, M., Williamson, R. S., & Shamsaei, N. (2018). Surface roughness effects on the fatigue strength of additively manufactured Ti-6Al-4V.

International Journal of Fatigue, 116, 543–552. doi:10.1016/j.ijfatigue.2018.07.013

Pearson, K. (1909). Determination of the Coefficient of Correlation. *Science, 30*(757), 23-25. doi:10.1126/science.30.757.23

Rott, S., Ladewig, A., Friedberger, K., Caper, J., Full, M., & Schleifenbaum, J. H. (2020). Surface roughness in laser powder bed fusion–Interdependency of surface orientation and laser incidence. *Additive Manufacturing, 36*, 101437.

Selema, A., Ibrahim, M., & Sergeant, P. (2022). Metal Additive Manufacturing for Electrical Machines: Technology Review and Latest Advancements. *Energies, 15*. doi:10.3390/en15031076

Sendino, S., Gardon, M., Lartategui, F., Martinez, S., & Lamikiz, A. (2020). The effect of the laser Incidence angle in the surface of L-PBF processed parts. *Coatings, 10*, 1024.

Senin, N., Thompson, A., & Leach, R. (2017). Characterisation of the topography of metal additive surface features with different measurement technologies. *Measurement Science and Technology, 28*, 095003. doi:10.1088/1361-6501/aa7ce2

Shubhavardhan, R. N., Weidong, L., Wenhan, Z., Tian, S., Paul, S., Xiang, J., & Shan, L. (2021). Surface Texture Characterization of Metal Selective Laser Melted Part With Varying Surface Inclinations. *Journal of Tribology, 143*(5), 1-37. doi:10.1115/1.4050455

Sneddon, S., Xu, Y., Dixon, M., Rugg, D., Li, P., & Mulvihill, D. M. (2020). Sensitivity of material failure to surface roughness: A study on titanium alloys Ti64 and Ti407. *Materials and Design, 200*(1). doi:10.1016/j.matdes.2020.109438

Sredanovic, B., Globocki-Lakic, G., Kramar, D., & Pusavec, F. (2018). Influence of workpiece hardness on tool wear in profile micro-milling of hardened tool steel. *Tribology in Industry, 40*(1), 100-107. doi:10.24874/ti.2018.40.01.09

Suh, C. H., Jung, Y. C., & Kim, Y. S. (2010). Effects of thickness and surface roughness on mechanical properties of aluminum sheets. *Journal of Mechanical Science and Technology, 24*(10), 2091–2098. doi:10.1007/s12206-010-0707-7

Thompson, A., Maskery, I., & Leach, R. K. (2016). X-ray computed tomography for additive manufacturing: a review. *Measurement Science and Technology,, 27*(7), 072001. doi:10.1088/0957-0233/27/7/072001

Tian, Y., Tomus, D., Rometsch, P., & Wu, X. (2017). Influences of processing parameters on surface roughness of Hastelloy X produced by selective laser melting. *Additive Manufacturing, 13*, 103-112.

Townsend, A., Senin, N., Blunt, L., Leach, R., & Taylor, R. (2016). Surface texture metrology for metal additive manufacturing: a review. *Precision Engineering, 46*, 34-47.

Wan, H. Y., Luo, Y. W., Zhang, B., Song, Z. M., Wang, L. Y., Zhou, Z. J., . . . Zhang, G. P. (2020). Effects of surface roughness and build thickness on fatigue properties of selective laser melted Inconel 718 at 650 °C. *International Journal of Fatigue, 137*, 105654. doi:10.1016/j.ijfatigue.2020.105654

Watring, D., Carter, K., Crouse, D., Raeymaekers, B., & Spear, A. (2019). Mechanisms driving high-cycle fatigue life of as-built Inconel 718 processed by laser powder bed fusion. *Materials Science and Engineering, 761*(5-8). doi:10.1016/j.msea.2019.06.003

Whip, B. R. (2018). *Effect of process parameters on the surface roughness and mechanical performance of additively manufactured alloy 718* . (Doctoral dissertation, Wright State University).

Wong, K. V., & Hernandez, A. (2012). A Review of Additive Manufacturing. *ISRN Mechanical Engineering*, 1-10. doi:10.5402/2012/208760

Yang, T., Xie, D., Yue, W., Wang, S., Rong, P., Shen, L., . . . Wang, C. (2019). Distortion of thin-walled structure fabricated by selective laser melting based on assumption of constraining force-induced distortion. *Metals, 9*(12), 1281.

Zeng, G. W., Monu, M. C., Lupton, C., Lin, B., & Tong, J. (2020). Towards a fundamental understanding of the effects of surface conditions on fatigue resistance for safety-critical AM applications. *International Journal of Fatigue, 136*. doi:10.1016/j.ijfatigue.2020.105585